CHARACTERIZATION OF METAL ORGANIC FRAMEWORK AND POLYMER
COMPOSITES AND THE METHOD OF THEIR PREPARATION

By

DHAYALAN ELANGOVAN

A THESIS

Submitted to
Michigan State University
In partial fulfillment of the requirements
For the degree of

MASTER OF SCIENCE

Packaging

2010

ABSTRACT

CHARACTERIZATION OF METALLIC ORGANIC FRAMEWORK AND POLYLACTIC ACID COMPOSITE AND THE METHOD OF THEIR PREPARATION

By

DHAYALAN ELANGOVAN

The research in this paper develops biodegradable functional polyester membranes based on poly(lactic acid) (PLA) and metallic organic frameworks (MOFs). PLA without and with the addition of 1, 3, and 5 w/w % MOF was melt compounded in a twin microextruder-compounder. Disc, rectangular and dumb-bell shaped samples were produced and their optical, physical, thermal, mechanical, thermo-mechanical and barrier properties were evaluated. The PLA and MOF composites showed poor interfacial adhesion between the PLA matrix and the MOF particles, which was previously predicted by using the Hansen's solubility parameters. The FTIR, UV and colorimetric studies showed selective absorption at particular wavelengths due to the presence of the MOF. The DMA results revealed that the heat deflection temperature (HDT), storage modulus, loss modulus and Tan Δ of the PLA/MOF composites did not change when compared to the PLA samples. However, there was a significant decrease in the brittleness of the PLA/MOF composite as evidenced by an increase of 15% in Izod impact strength and of 170% in elongation at break with respect to the PLA control samples. The permeability of PLA/MOF composite films to oxygen and water did not change when compared to the neat PLA film. However, the sorption capacity of the PLA/MOF composites films increased up to two fold at each relative humidity to which the films were exposed. The sorption and desorption curves of the PLA/MOF composite films showed a hysteresis phenomenon.

ACKNOWLEDGEMENTS

TABLE OF CONTENTS

LIST OF TABLES

LIST OF FIGURES

CHAPTER 1. INTRODUCTION

The concerns related to environmental pollution caused by non-biodegradable polymers are increasing. As a consequence, researchers are developing polymers with a lower environmental footprint from biobased resources for potential use in packaging. Among the various commercially available biobased and/or biodegradable polymers such as poly(hydroxybutyrate) (PHB), poly(butylene adipate-co-terephthalate) (PBAT), poly(tetramethylene adipate-co-terephthalate) (PTAT), and poly(ε-caprolactone) (PCL), poly(lactic acid) (PLA) is one of the most used and promising biopolymers that has drawn commercial attention in recent years due to its compostability, high mechanical strength, high transparency, good processability, and water solubility resistance [1, 2].

PLA has been used in a number of biomedical applications and drug delivery devices. Some of these applications include implants, sutures, and drug encapsulation [3]. It has been approved as GRAS (generally regarded as safe) for use in contact with food [4], and it is currently used for packaging fresh produce, bottled water, juices, yogurt, and disposable tableware in Japanese, European and North American markets [5]. In the form of fibers and non-woven textiles, PLA also has many potential uses, for example as upholstery, disposable garments, awnings, feminine hygiene products, and diapers [6].

The use of PLA containers for food and medical packaging has increased. It is necessary for the container/package to protect the product by functioning actively throughout the product shelf life by providing, for example, active or selective barrier properties. In the packaging industry, several means of regulating the exposure of product to gases have already been developed, including modified atmosphere packaging (MAP) and active packaging. In the case of active packaging, the inclusion of scavengers in the form of sachets within the cavity or

1

interior of the package is one of the most common and accepted practices. One disadvantage of sachets is the need for additional packaging operations to add the sachet to each package, and the end disposal of the system. A further disadvantage arising from the use of some sachets is that certain atmospheric conditions (e.g., high humidity, low CO_2 level) in the package are required in order for scavenging to occur at an adequate rate.

Another means of limiting the exposure of product to gases involves incorporating a functional membrane into the packaging structure itself. By incorporating the scavenging material in the package itself, a more uniform scavenging effect throughout the package can be achieved. In addition, such incorporation can provide a means to restrict and scavenge gases and moisture as they pass through the walls of the package (referred to as an "active" or "functional" barrier), thereby maintaining the lowest possible gas and moisture level throughout the package [7]. Adsorbents are the materials used to modify the packaging material in order for the package to function actively by adsorbing gases and moisture.

The most commonly used adsorbents are zeolites, activated carbon, silica gel, and alumina [8, 9]. These materials are being used to modify polymer properties in order to increase the absorbent capacity for water and other compounds such as gases, vapor, and liquids to permit its use as a functional membrane in industrial applications. The surface area of these added compounds largely determines the absorbent capacity of the particular material when it is combined with the polymers. The main disadvantage of these materials is their limited surface area, resulting in reduced absorbent capacity. Moreover, it is not possible to tailor their structures based upon the requirements for particular applications, and it is impossible to increase the surface of these materials, without altering the dead volume of the adsorbant.

To overcome the defects of the current adsorbent materials, researchers have developed novel compounds named metal organic framework (MOF) materials, which are crystalline compounds consisting of metal ions (copper, zinc, aluminum, etc.) or clusters coordinated to rigid organic molecules to form one-, two-, or three-dimensional structures that can be porous. MOFs have a surface area between 1000 and 3000 m^2/g or more, which is equivalent to a football field. This surface area is close to one order of magnitude higher than that of zeolites and activated carbon [10, 11]. Besides the increased surface, they also have open internal structures and long-range crystallinity. Their distinctive pore sizes can accommodate different types of gases such as CO_2, O_2, N_2, CH_4 and other small volatile organic compounds (VOCs).

To make use of the distinctive properties of MOFs and the versatile nature of PLA, the main goal of this research is to compound poly(L lactic acid) (PLLA) with MOF particles to produce functional polymeric membranes. The new PLLA/MOF functional membranes are expected to have novel properties that cannot be obtained when modified with other adsorbent materials. Thus, the main objectives of this thesis are to:

- Characterize PLLA for its solubility parameters, contact angle and its molecular weight;
- Characterize the surface area, density and pore size of MOF;
- Develop PLLA/MOF composite sample films by melt compounding using a twin screw extruder;
- Evaluate PLLA/MOF composite samples for their optical, physical, mechanical, thermo-mechanical, and barrier properties, and their sorption to water and organic compounds.

REFERENCES

4

REFERENCES

1. V. Siracusa, P. Rocculi, S. Romani. M.D. Rosa, "*Biodegradable polymers for food packaging: a review",* Trend in Food Science and Technology, 19(12), 2008, pp. 634-643.

2. J. Ahmed, S.K. Varshney, J.X. Zhang, H.S. Ramaswamy, "*Effect of high pressure treatment on thermal properties of polylactides*", Journal of Food Engineering 93(3), 2009, pp.308-312.

3. L. Avérous "*Polylactic acid: synthesis, properties and applications" In "Monomers, Polymers and Composites from renewable resources*", Eds: Belgacem N. et Gandini A., Elsevier Limited Publication. Chap. 21, 2008, pp. 433-450.

4. T. Jin, H. Zhang, "*Biodegradable polylactic acid polymer with nisin for use in antimicrobial food packaging*", Journal of Food Science, 73(3), 2008, pp. M127–M134.

5. Mutsuga, M., Kawamura, Y., Tanamoto, K., "*Migration of lactic acid, lactide and oligomers from polylactide food-contact materials*", Food Additives and Contaminants 25(10), 2008, pp. 1283–1290.

6. Ke, T., Sun, X.S., "*Thermal and mechanical properties of poly(lactic acid)/ starch/methylenediphenyl diisocyanate blending with triethyl citrate*". Journal of Applied Polymer Science 88(13), 2003 pp. 2947–2955.

7. T.Y. Ching "*Oxygen Scavenging ribbons and articles employing the same*", US Patent No.5744246, 1998.

8. R.T. Yang, "*Adsorbents: Fundamentals and Applications*", John Wiley and Sons, May 2003.

9. I.E. Yuzay, R. Auras, S. Selke, "*Poly(lactic acid)/Aluminum Oxide Composites Faricated by Sol-Gel and Melt Compounding Process*" Macromolecular Materials and Engineering, 295(3), 2009, pp.283-292.

10. The BASF chemical company, "*BASOLITE metallic organic framework data sheet*", June 2008. Available at "http://www.catalysts.basf.com/Main/adsorbents/basf_adsorbent_technologies/metal_org anic_frameworks".

11. Mueller et al. "*Metal–organic frameworks—prospective industrial applications*", Journal of Materials Chemistry, 16, 2006, 626-636.

CHAPTER 2. LITERATURE REVIEW

Plastics are widely used in packaging due to their distinct features such as softness, lightness and transparency [1]. According to Kolybaba *et al*. [2] three classes of polymeric materials are currently studied for their applications in packaging and other related fields: 1) conventional, 2) partially degradable, and 3) completely biodegradable polymers.

Most of the conventional plastics are not biodegradable [3]. Microorganisms present in the soil or other natural environments are not able to consume portions of the plastic and that makes them non-biodegradable. This group of materials contains an impenetrable matrix, which could be reinforced with fillers such as carbon or glass fibers, and in general they are petroleum-based.

The second class of polymeric materials under investigation is partially degradable. They are of similar origin as conventional plastics but designed with the goal of more rapid degradation. These materials are produced from petroleum or biomass resources. They can also be reinforced with different fillers. Once the products are disposed, the microbes partly digest the macromolecules in the polymer matrix. Once the macromolecules are consumed the weakened material undergoes further degradation until it is totally degraded.

The final type of polymer, which is getting attention from researchers and industries, is polymers that are biodegradable and/or compostable. These plastics can be also obtained from petroleum and/or renewable resources. The renewable resources used to derived these types of polymeric materials are crops such as corn, sugar beets, and stratch; also, they can be obtained from petroleum resources with polymers with preferred degradable chemical structures such as poly(butylene-co-adipate-terephthalate) and poly(ε-caprolactone). These materials can be

completely consumed by microorganism, leaving carbon dioxide, humus, and water as by-products, or they can be composted under specific conditions [2, 6, and 7].

Due to their lower cost and some higher performance factors like good tensile and tear strength, good barrier to oxygen, carbon dioxide, water and aroma compounds, and heat sealability, packaging is dominated by petroleum based polymers such as polyethylene (PE), polypropylene (PP), polyethylene terephthalate (PET), polystyrene (PS), and poly(vinyl chloride) (PVC), among others [16]. The United States is the largest producer and holds the largest market for thermoplastic materials. From 1997 to 2001, the growth in sales of thermoplastics for packaging materials was 4.2% and that of consumer and institutional application was about 2.0%. Overall increase in the growth rate of thermoplastics across all the markets was 3.0% over the same period [4, 5].

Despite their appreciable advantages over other types of packaging materials, petroleum based polymers are made from non-renewable resources, which is an increasing concern for manufacturers and the public in general. Packaging plastic waste has led to a serious ecological threat, and they are getting accumulating in landfills. Increase of recycling and recovering of polymers could reduce the amount of plastics sent to landfills. In the last decade, special attention has been given to compostable plastics. Therefore, new packaging materials produced from renewable and non-renewable resources that can be recovered through biodegradation and/or composting are being developed and studied.

The American Society for Testing of Materials (ASTM) and the International Standards Organization (ISO) define degradable plastic "as those which undergo a significant change in chemical structure under specific environmental conditions" [8]. Biodegradable polymers disposed to the environment undergo degradation from the action of naturally occurring

7

microorganisms such as bacteria, fungi and algae. Some of the plastics can also be degraded by light (photo degradable), oxidation (oxidatively degradable), and hydrolytic activity (hydrolytically degradable). Biodegradable plastics are generally broken down within a few months to 2 years under bioactive conditions (i.e., environments in which microorganisms are active).

The standard specifications and terminologies required to address the compostability of plastic materials is defined in ASTM D6400, and the procedure used to test the mineralization of plastic materials is described in ASTM D5338. ASTM D6400-04 defines compostable plastic as "a plastic that undergoes degradation by biological processes during composting to yield carbon dioxide, water, inorganic compounds, and biomass at a rate consistent with other known compostable materials and leaves no visually distinguishable or toxic residues". ASTM D5338 is used to determine the mineralization of the biodegradable plastic under simulated or controlled composting condition. To pass the disintegration, biodegradation and ecotoxicity requirements the following criteria should be met: 1. After sieving the final compost, the fraction of plastic material which has size greater than 2 mm should not be more than 10%, 2. The mineralization must be greater than 60% for homopolymers and random copolymers or 90% for block/graft copolymers or blends, 3. The concentration of heavy metals in the materials should be less than 50% as described in 40CFR #503.13. 4. The compost obtained from the degradation of the polymer should be able to support plant growth for at least two species [9-11].

The growing need for materials that can substitute for conventional plastics has led to the development of biodegradable plastics for packaging applications. Biodegradable plastics have already found large application in the field of medicine. For example, poly (lactic acid) (PLA) has been used in biomedical applications since the 1970s. Due to its higher cost, there was not

considered for other applications where cheaper options were already available with conventional plastics [12].

Figure 2.1 shows the classification of biodegradable polymers according to Averous *et al.* The four different classifications of polymers are 1) obtained from biomass, 2) obtained by microbial production, 3) chemically obtained by using biomass based resources, and 4) obtained from petroleum resources [13].

Many biodegradable plastics are used in packaging applications, but they always lag behind conventional plastics due to their cost and some performance factors. As higher volumes of these polymers are being produced, the cost and the challenges of performance are being solved. Many of these biodegradable polymers, such as PLA, poly(hydroxy butyrate) (PHB), aliphatic aromatic co polyesters like poly(butylene adipate-co-terephthalate) (PBAT) and poly-(tetramethylene adipate-co-terephthalate) (PTAT), poly (ε-caprolactone) (PCL), poly(butylene succinate) (PBS), and cellulose based polymers are entering the field of packaging. Among these, one of the most promising biopolymers is PLA, which is widely used in packaging applications such as films, thermoformed cups and clamshells, and bottles [4, 14].
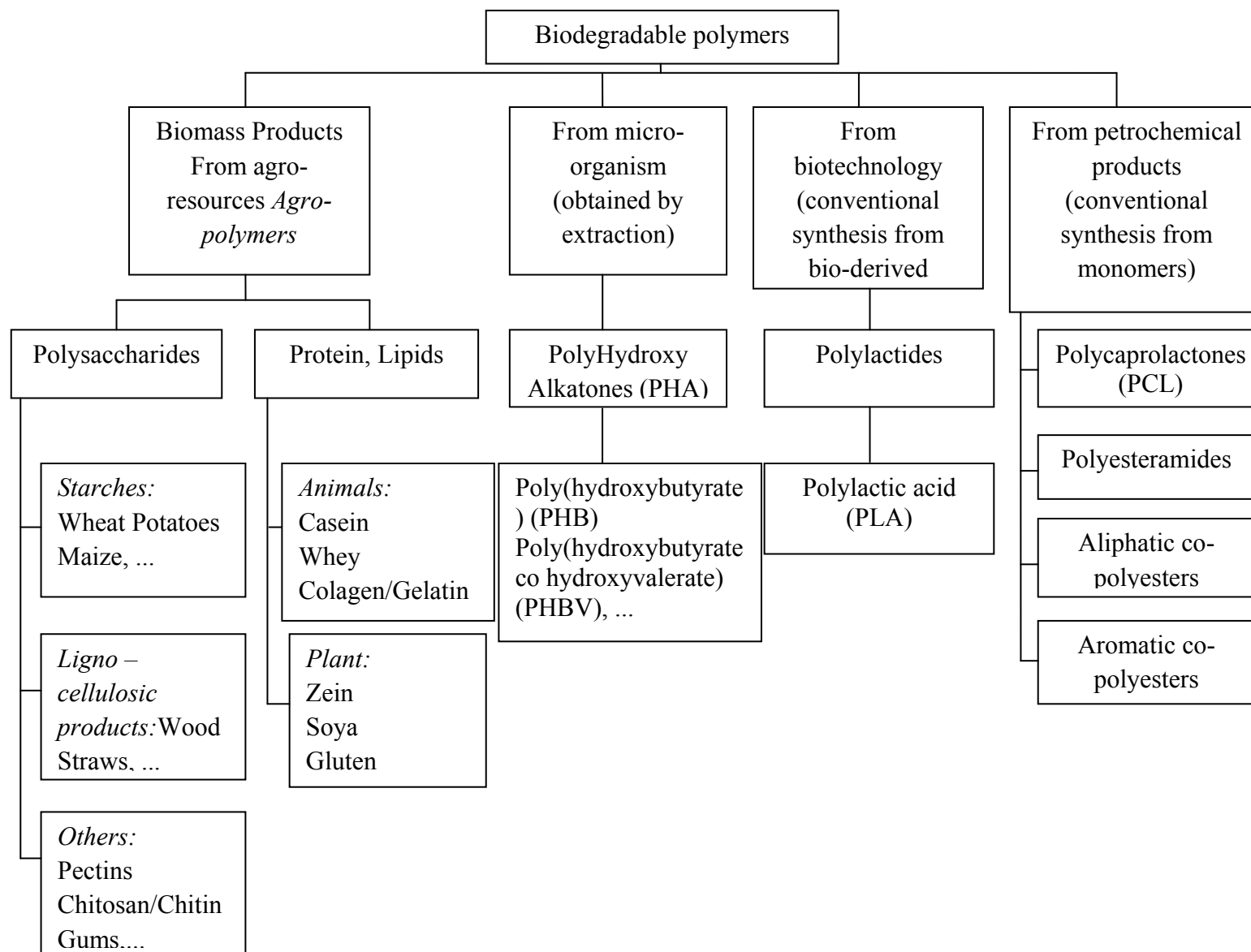
Figure 2.1 Classification of the biodegradable polymers, (adapted from Averous' *et al.* [13])

Poly(lactic acid), PLA

PLA is not a new material since it was developed in 1932 by Carothers and then later by Dupont and Ethicon. Nowadays, PLA is made from 100% annually renewable resources like corn and sugar beets and has the potential for commercial large-scale production and applications in packaging. It exhibits good transparency, and processability with increased molecular weight. It can be also recycled or composted. It is a stiff and rigid thermoplastic that can be totally amorphous or semi-crystalline depending on the stereochemistry of the polymer backbone. D-lactic acid monomers are incorporated to modify the crystallization behavior to have certain properties and applications. This modified flexible PLA can be used to make a wide variety of packaging materials [4, 5, 15, and 16].

PLA can be produced with high molecular weight ranges by different techniques. For example, NatureWorks LLC uses ring opening polymerization technique followed by a novel distillation method, whereas Mitsui Toatsu uses the solvent based process with azeotropic distillation to convert the lactic acid into high molecular weight PLA [4]. It has been reported that commercial PLA can be prepared by two kinds of methods, viz. direct condensation of lactic acid and ring opening polymerization (ROP) of the cyclic lactide dimer (Figure 2.2) [15].
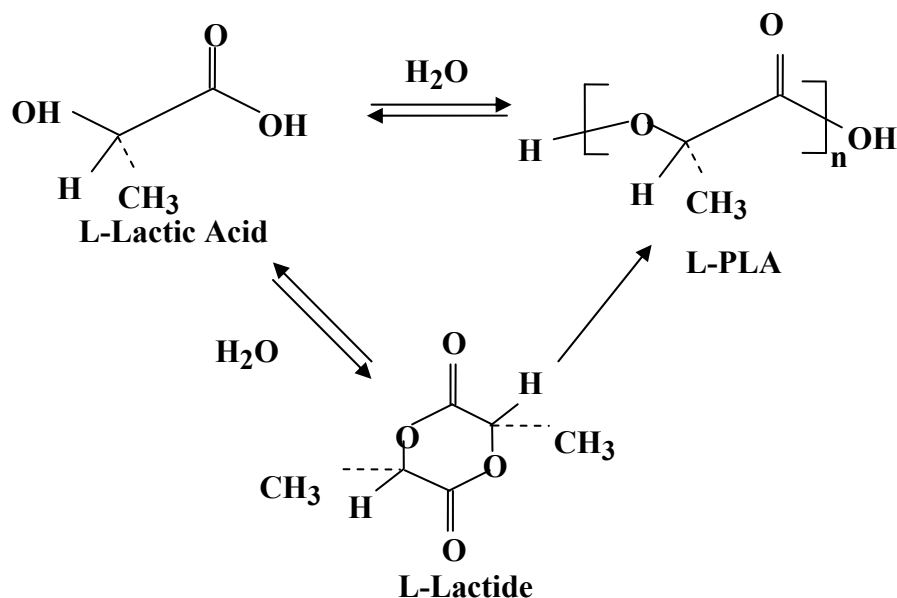
Figure 2.2 Polymerization routes to polylactic acid, (adapted from Drumright *et al.*[15])

However, most of the production is based on the latter method, *i.e.*, ROP. Cargill Dow developed and patented a low-cost continuous process that is based on the melt method rather than the solution one and is solvent free with substantial economic and environmental benefits. In this process, a pre-polymer of low molecular weight PLA is produced first by the continuous condensation process of aqueous lactic acid. Then, to increase the rate and selectivity of the intramolecular crystallization reaction, using tin catalyst, the PLA prepolymer (around 1,000 Da) is depolymerized into a mixture of lactide stereoisomers, which is then purified by vacuum distillation. Finally, the high molecular weight PLA is produced through the ROP of those lactides in the melt form using the tin catalyst again and thus avoiding the use of the costly and non-eco-friendly solvents (Figure 2.3) [15]. After the polymerization, any remaining monomer is removed under vacuum and recycled to the beginning of the process (Figure 2.4) [13].

Figure 2.3 Schematic of PLA via prepolymer and lactide, adapted from Drumright *et.al* [15].

Figure 2.4 Nonsolvent process to prepare polylactic acid, adapted from *chemical weekly* [17].
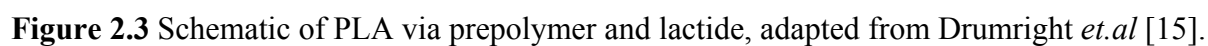
Environmental footprint of PLA

In recent years, demands for sustainability in products, processes and technology have increased. Process or products that use large quantities of energy, cause pollution to the environment, or emit more greenhouse gases are considered to be less sustainable. Green chemistries are processes that use novel chemical techniques to create products that are less harmful to the environment and also to make those products commercially viable. A common established method to quantify the environmental footprint of products or processes is life cycle assessment (LCA). It looks at all factors of the product or process from the raw material to end-use and disposal. The use of energy, pollution of air and water, as well as the hazards of the chemicals used to develop the product or processes are assessed against alternate products or solutions.

According to Cargill Dow LLC, their PLA production process (1) prevents pollution at the source by using lactic acid produced by natural fermentation process, (2) substitutes annually renewable materials for petroleum based feedstock, (3) avoids the use of solvents or other hazardous materials, (4) recycles product and by-product streams and (5) uses catalysts to reduce energy consumption and to improve yield. In addition, PLA can be either recycled or composted [4]. Cargill Dow stated that PLA produced by them uses from 20 to 50% less fossil fuels than conventionally available plastic resins (Figure 2.5). This means that up to 2 to 5 times more PLA can be produced with the same amount of fossil fuel than the petrochemical-based plastic resins. The ability to produce the polymer on a favorable cost/performance basis is critical to realize these benefits. This can be achieved through efficient use of raw materials, reduced use of energy, and elimination of solvents.

14

CO_2 is one of the greenhouse gases that contribute to climate change, and CO_2 measurements can serve as indicators of the carbon footprint of materials and processes. According to Gruber [18], PLA has a very low impact on CO_2 emission since the CO_2 generated during PLA biodegradation is balanced by the equal amount of CO_2 taken from the atmosphere during the growth of plant feedstocks. Figure 2.6 shows the CO_2 emission contribution to the environment for common plastic products [4, 18]. In 2006, PLA production emitted about 0.27 kg CO_2 eq/kg of PLA (Figure 2.7) and the fossil energy used was 27.2 MJ/kg PLA (Figure 2.8). This represents about 85% and 50% reduction in CO_2 emission and fossil energy use, respectively, when compared to the PLA production in 2003 [19].
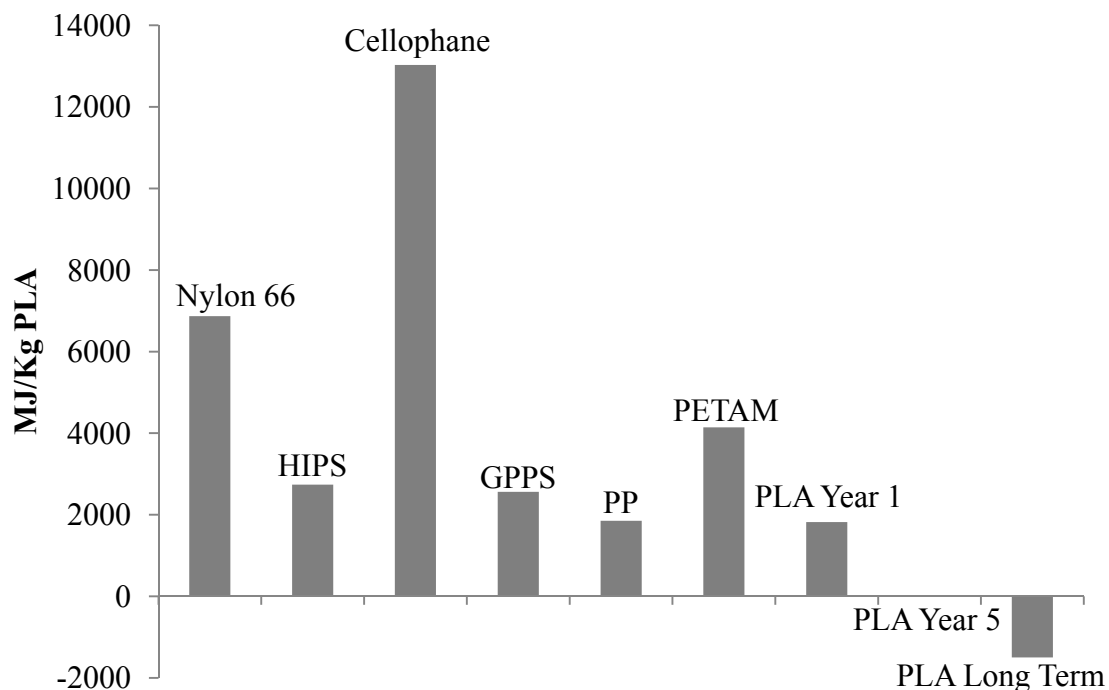
Figure 2.5 MJ/Kg of energy required to produce various polymers, adapted from Gruber [18]. The Cargill Dow products are "PLA year 1, PLA year 5, PLA long tem" ("For interpretation of the references to color in this and all other figures, the reader is referred to the electronic version of this thesis.")
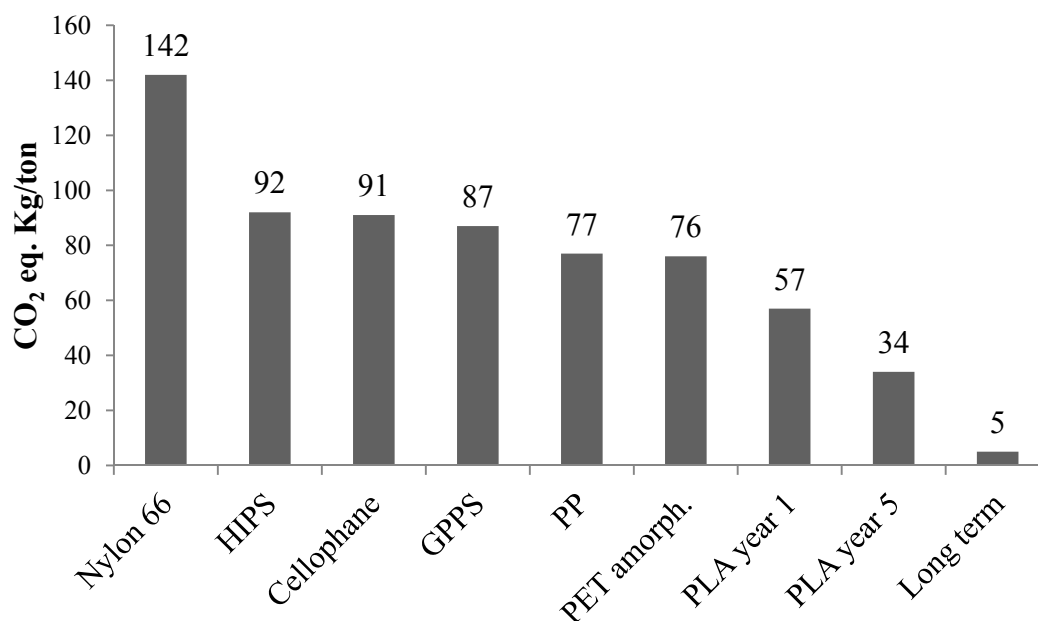
Figure 2.6 CO_2 emissions (kg/ton) resulting from production of various polymers, adapted from Mohanty *et al.* [4]. The Cargill Dow products are "PLA year 1, PLA year 5, PLA long term" ("For interpretation of the references to color in this and all other figures, the reader is referred to the electronic version of this thesis.")
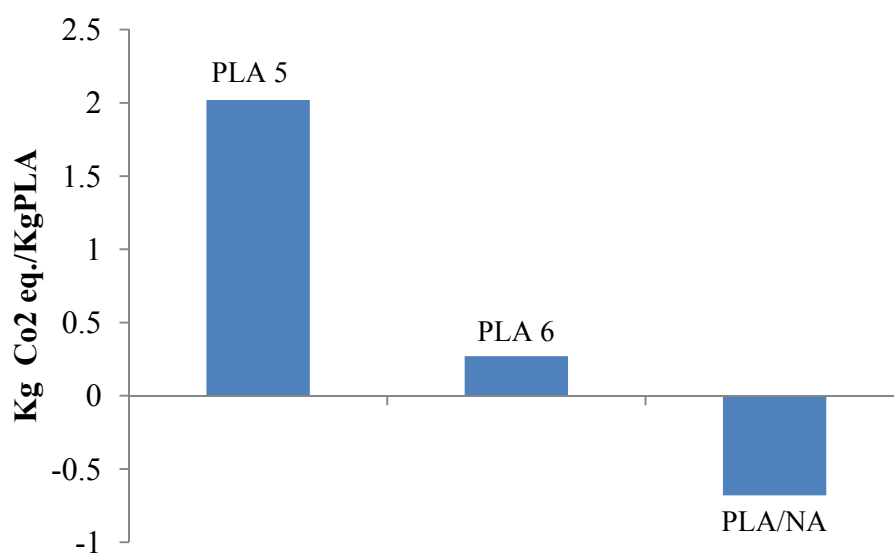
Figure 2.7 Cradle-to-polymer-factory-gate greenhouse gas emissions for PLA year 5 (PLA 5), PLA year 6 (PLA 6) and PLA long term (PLA NA), adapted from Vink *et.al* [18]. ("For interpretation of the references to color in this and all other figures, the reader is referred to the electronic version of this thesis.")
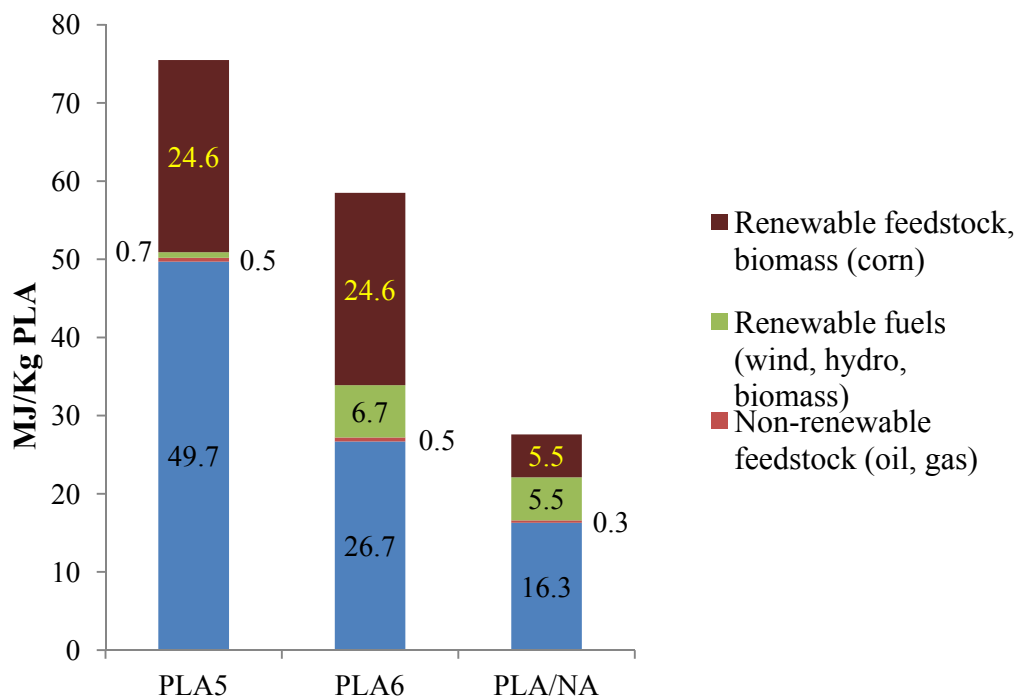
Figure 2.8 Cradle-to-polymer-factory-gate gross energy use for PLA year 5 (PLA 5), PLA year 6 (PLA 6) and PLA long term (PLA NA), adapted from Vink *et.al* [18]. ("For interpretation of the references to color in this and all other figures, the reader is referred to the electronic version of this thesis.")

PLA properties

Stereochemistry of PLA is very important in the final polymer's thermal behavior, and its mechanical properties and thermo-mechanical performance. PLA can be made from three kinds of stereo isomers: L-lactide, D-lactide and meso-lactide. PLA has a melting point (T_m) of around 180°C with an enthalpy of 40-50 J/g; however, for the semi-crystalline PLA, depending on the structure, the range is from 130-230°C and the glass transition temperature (T_g) is about 58°C. An enthalpy of fusion of 93.1 J/g is reported for the 100% crystalline PLLA and PDLA homopolymers that have "infinite" crystal thickness [5, 15].

17

Pure crystalline PLLA has an estimated density range of 1.37-1.49 g/cc, and solid amorphous PLA has a density of about 1.25g/cc. The incorporation of other lactic acid monomers in this mostly naturally produced PLLA will affect its stereochemistry, crystallization, and other properties, although there will be little effect on T_g. It is also possible to derive purely amorphous PLA by incorporating about 15% of meso-lactide monomers. It has been reported that the optimized crystallization temperature (T_c) is in the range of 105-115ºC [5, 15].

Based on the above PLA chemical structures, it is possible to make various kinds of PLA resins that can be used to produce blown films, cast films, biaxially oriented films, injection molded or blow molded articles, etc. By controlling certain process parameters at the molecular level such as branching, molecular weight distribution (MWD), D-isomer content and branching introduction and by incorporating the L-, D- and meso lactide isomers at various levels in the PLA back bone, PLA can be tailored for specific applications. PLA has excellent gloss and transparency and the tensile properties are similar to PET. PLA provides a good barrier for aromas and flavors, low temperature sealability, and good crease retention and crimp properties. These make PLA a good choice as a packaging material. Table 2.1 provides some experimental data for some properties of PLA [1].

Table 2.1 Physical properties of PLA, adapted from Siracusa *et al.* [1]

Experimental Data	PLA
T_g(ºC)	62.1±0.7
T_m(ºC)	150.2±0.5
Percent crystallinity (X_c)	29.0±0.5
Oxygen transmission rate (OTR) (cc/m² day)[a]	56.33±0.12
Oxygen permeability rate (OPC) (kg m m⁻²s⁻¹Pa⁻¹)[b]	1.21E-18±0.07E-18
Water vapour transmission rate (WVTR) (g m⁻² day⁻¹)[a]	15.30±0.04
Water vapour permeability rate(WVPC) (kg m m⁻²s⁻¹Pa⁻¹)[c]	1.89E-14±0.08E-14
[a]Thickness of 20.0±0.2 mils [b] OPC= OTR x l/ΔP, where l is the thickness in m and ΔP is the difference in oxygen partial pressure across the film. [c]WVPC= WVTR x l/ΔP, where l is the thickness in m and ΔP is the difference in water vapour partial pressure across the film.	

PLA possesses intermediate water vapor barrier properties and is not as affected by RH as in the case of nylon. Combined with its relatively intermediate oxygen barrier properties, this makes it one of the favorable materials for food packaging. It was found that the O_2:CO_2 permeability ratio of PLA is in the range of 1:7 to 1:12, which makes it suitable for food packaging where high respiration is needed [14, 16].

The mechanical properties of PLA are comparable to those of conventional polymers such as PE and PS. PLA has better barrier properties than PS but lower than PET. The physical properties of PLA are similar to those of PS but not as good as those of PET [16, 21].

Although PLA has properties comparable to those of conventional polymers, its brittle nature dramatically reduces its application in packaging. Toughening of PLA can be achieved through plasticization, incorporation of its own isomers during polymerization, or blending PLA

with tough polymers. Many studies are underway to improve the toughness of PLA [14]. Many combinations of blends of PLA with nanocomposites materials have investigated in order to increase the mechanical, thermo-physical, and barrier properties of the PLA films [22].

Polymeric biocomposites are materials formed by a biodegradable matrix (resin) of synthetic or natural origin and a reinforcing phase. PLA biocomposites have been used for medical applications and in the field of structural plastics. In biomaterials, each and every compound of the composite should be biocompatible. Also, the interface between compounds should not be affected by the body environment. Normally, biocomposite materials can be classified into three groups: 1) particulate composites, 2) fibrous composites, and 3) porous composites [23].

Although PLA has undergone remarkable developments for its application in medical-based devices, there are still demands to increase the mechanical performance of medical implants and also their bioactivity. This is normally done by optimizing the amount of fillers such as zirconia, magnesium oxide, hydroxyapatite, and carbon fibers in selected groups of biodegradable polymer matrices [23-25]. For example, PLLA composite with 10 % w/w of filler increases the stiffness of the material but decreases the tensile strength of the material by 30% [26]. In the case of PLLA-clay composites, the Young's modulus of the material increases with increased clay addition levels at filler content below 10 % w/w [27].

Huda *et al.* [31] compared the properties of PLA composites made with reinforcing glass fiber to those made with recycled newspaper cellulose fiber by using a twin screw extruder and an injection molding system. The mechanical and thermo-physical properties of the PLA/recycled newspaper composite were similar to those of PLA/glass fiber composite. This

study suggests that PLA/recycled newspaper composites can be potentially useful technology to replace PLA/glass composites when very high load bearing requirements are needed.

In addition to macro-scale particles, PLA has been compounded with nano-scale particles to improve the mechanical, barrier and thermal properties. Some of the nano-particles include layered silicates, carbon nanotube, hydroxyapatite, layered titanate, and aluminum hydroxide [29, 30]. According to Thellen *et al* [31], Montmorillonite (MMT)-PLA composite has a 50% increase in the oxygen barrier properties and a 20% increase in the storage modulus when compared to neat PLA.

Porous colloidal particles have attracted renewed interest, from both fundamental and applied research prespectives. The large internal surface area and adsorbent potential of porous particles have led to their widespread application in diverse fields, including sensing, catalysis, and drug delivery. These compounds include zeolite, activated carbon, silica and metal organic framework (MOF). Porous polymeric membranes are also used in membrane separation process of gases and liquid due to its adsorption capacity [33].

The accumulation of atoms and molecules on the surface of a material is called adsorption, which is different from absorption where the substance diffuses to form a solution. During adsorption, the atoms, which are on the material's surface, are not fully covered by their closest neighbors, which helps to attract other atoms or molecules and thus the surface energy can be decreased [34].

Adsorbates can bond to the surface of the material in a variety of ways. These include: 1) ontop site, in which the adsorbate forms a single bond with only one atom beneath it; 2) bridging site, in which the adsorbate forms two bonds between the two surface atoms; and 3) hollow site, in which the adsorbate bonds with three or more atoms. Depending on the nature of the bonding,

21

the adsorption process can be classified into physical adsorption or physisorption (Van der Waals bonding) and chemical adsorption or chemisorption (covalent bonding). The materials used to promote adsorption are called adsorbents [34].

Adsorbents are usually pellets, rods, moldings, or monoliths having 0.5, 10 mm, etc. hydrodynamic diameter. Due its greater abrasion resistance, thermal stability combined with tiny pore size the adsorbents exhibit increased surface area, which in turn increases its capacity to adsorb solvents and gases. The adsorbents should also have a distinct pore size to make them good candidates for transport of gaseous vapor [35].

The industrial adsorbents are classified into three major categories: 1) compounds based on oxygen, which are polar and hydrophilic (e.g. silicia gel and zeolites); 2) compounds based on carbons, which are hydrophobic and non-polar (e.g. activated carbon and graphite); and 3) compounds which are polymer-based, having polar or a-polar functional groups in the polymer matrix which are porous [35]. Adsorbents are used in a variety of fields including medical, petrochemical industry, nuclear industry, agriculture, animal welfare, heating and refrigeration, detergents, construction, gemstones, aquarium keeping, and space hardware testing. The most commonly used adsorbents in the science and technology field are zeolites, activated carbon, alumina, and silica gel [38].

Zeolites are microporous crystalline aluminum silicate minerals of alkali or alkali earth metals such as sodium, potassium, and calcium. Zeolites are commercially used as adsorbents and belong to the family of microporous solids known as "molecular sieves". The primary building blocks of zeolites are the tetrahedral structural units of silicon and aluminum oxide (SiO_4 and AlO_4). The tetrahedral structure of the zeolites can be assembled in different ways, making it possible to fabricate some 800 crystalline structures. Substituting other elements in

place of Al and Si in the framework of zeolites can result in numerous varieties of molecular sieves. The main interest of the petrochemical industry in zeolite materials is their 12-membered oxygen rings with a diameter of 8.1Å, which will prohibit large hydrocarbon molecules from penetrating. Zeolites are used as catalysts in the petrochemical industry and other applications include molecular separation, water purification, and active packaging [36-40].

Another common adsorbent material is activated carbon, also called activated charcoal or activated coal. It is a form of carbon that is processed to obtain large micropore and mesopore volumes and a high surface area. One gram of activated carbon has a surface area of about 500 m^2/g as measured by nitrogen adsorption. The pore size of activated carbon varies from Angstrom to micrometer, which makes activated carbon useful for numerous applications. Activated carbons with micropores have found application in gas adsorption, and those with mesopore structures are used for adsorption of larger molecules. Other applications of activated carbon include gas purification, solvent recovery, and wastewater treatment [38, 41].

Activated alumina is crystalline amphoteric oxide of aluminum, with the chemical formula Al_2O_3. It is widely used as a desiccant due to its large capacity to store water. The geometry of the pores and the surface chemistry can be altered by treating with acid or alkaline solutions and also by controlled thermal treatment. This makes activated alumina more useful than silica gel, so it is used as a sorbent material. These materials are also used as oxide ceramics due to their excellent hardness, corrosion resistance, and ease of processing [38, 42].

Silica gel as a drying agent is extensively used in dehumidification processes because of its high moisture adsorption capacity and large surface area. It can store water up to 40% of its weight, and it is easier to regenerate than zeolites. To regenerate, zeolite requires a temperature of 350°C, but silica gel requires only 150°C. Its surface can be modified by grafting with a

monomolecular layer of organic ligand. Silica gels thus modified are being increasingly used for chromatography applications [38, 43].

Adsorbents are also being used to modify polymer properties in order to increase the adsorbent capacity for water and other compounds such as gases, vapor, and liquids for use as functional membranes in industrial applications. In recent years, metal organic frameworks (MOF) have been widely used in catalysis, gas separation and storage. Compared to zeolites, carbon, alumina and silica gel the MOF provides more flexibility to control its design and functionality [44, 45].

Metal Organic Frameworks (MOF)

"Metallic Organic Frameworks (MOFs) are crystalline compounds that contain metal ions or clusters coordinated to rigid organic molecules to form one-, two-, or three- dimensional structures that can be porous" [47]. A general comparison of MOFs with other available adsorbent materials is found in Table 2.2. [46].

Table 2.2 MOF Performance Comparison, adapted from *BASOLITE MOF Datasheet* [46]

Current Technology	MOF performance comparison
Zeolite	MOF have close to an order of magnitude higher surface area and no dead volume, high uptake capacity, low desorption energy, and structural variety. Metal atoms are atomically dispersed for catalytic activity.
Silica	MOF have significantly higher surface areas and high uptake capacity.
Alumina	Hydrophilic MOF are available with more than one order of magnitude higher surface area, low desorption energy, reversibility and stability against water.
Activated Carbon	An organophilic MOF (Z1200) is available with even higher surface area, can be reactivated, and is stable at high temperatures. Custom tailored structures possible in the future.

The surface area of MOFs is close to one order of magnitude higher than that of zeolites and activated carbon. [46] Besides the increased surface, they also have open internal structures

and long-range crystallinity. MOFs with high surface areas and porosity to have promising properties for high adsorption capacities of various gases. HKUST-1 (copper benzene tricarboxylate) was first reported by Williams *et al.,* [48] and subsequently studied by numerous research groups. MOF contain metal sites in their walls where coordination to a gas molecule can take place [49].

According to Muller *et al.* [47], the storage of transportation fluids using porous compounds can be a useful technology for the automobile industry. MOF's increased surface area combined with low energy adsorption capacity of gas increases the storage capacity of the cylinder filled with MOF roughly twice when compared to standard cylinders. MOFs are made of two important components: a linker (organic molecule) and a metal ion (in some cases a cluster of metal ions). Mono-, di-, or tri- ligands usually make up the organic units. [45] Based on the metal and linker the properties and structure of MOFs will be different. For example, the coordination preference of different metals will determine the geometry of the pores and the number of ligands that can be bound to the metal and orientation. Table 2.3 lists the common ligands that have been used in MOFs. [50]

Table 2.3 Common ligands (linkers) in MOFs, adapted from David *et.al* [50]
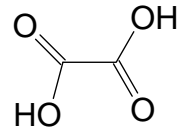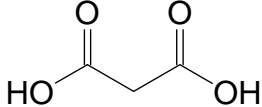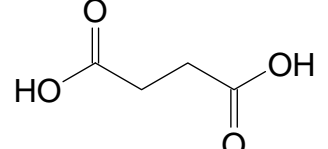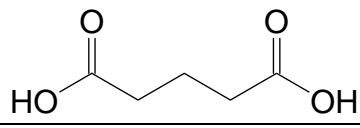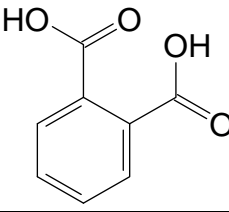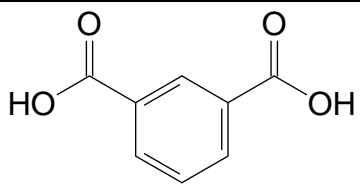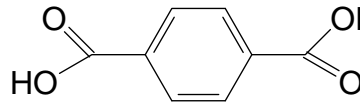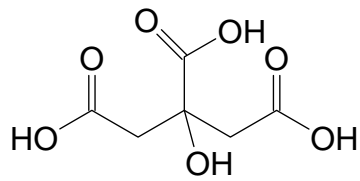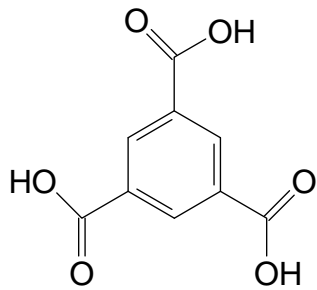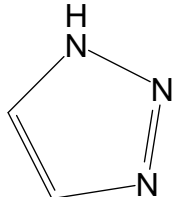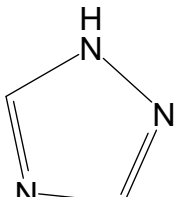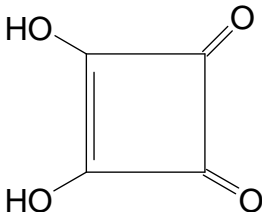
Common name	IUPAC name	Chemical formula	Structural formula
Oxalic acid	ethanedioic acid	HOOC-COOH	
Malonic acid	propanedioic acid	$HOOC-(CH_2)-COOH$	
Succinic acid	butanedioic acid	$HOOC-(CH_2)_2-COOH$	
Glutaric acid	pentanedioic acid	$HOOC-(CH_2)_3-COOH$	
Phthalic acid	benzene-1,2-dicarboxylic acid *o*-phthalic acid	$C_6H_4(COOH)_2$	
Isophthalic acid	benzene-1,3-dicarboxylic acid *m*-phthalic acid	$C_6H_4(COOH)_2$	
Terephthalic acid	benzene-1,4-dicarboxylic acid *p*-phthalic acid	$C_6H_4(COOH)_2$	
Citric Acid	2-Hydroxy-1,2,3-propanetricarboxylic acid	$(HOOC)CH_2C(OH)(COOH)CH_2(COOH)$	

Table 2.3 Cont'd

Trimesic acid	benzene-1,3,5-tricarboxylic acid	$C_9H_6O_6$	
1,2,3-Triazole	1H-1,2,3-triazole	$C_2H_3N_3$	
pyrrodiazole	1H-1,2,4-triazole	$C_2H_3N_3$	
Squaric acid	3,4-Dihydroxy-3-cyclobutene-1,2-dione	$C_4H_2O_4$	

MOF and zeolites are synthesized by growing crystals slowly from metal precursors such as metal nitrates and organic ligands. This type of synthesis mechanism is called the hydrothermal or solvothermal technique. The structure directing compounds used to formulate zeolites are also used for the formulation of MOF. The solvents water and N, N-diethylformamide have been used to produce MOF for gas storage purposes. This type of synthesis allows metal sites to expose completely, which allows hydrogen to bind to the sites [53].

A typical MOF synthesis flowchart, indicating the different steps of MOF preparation, as well as recycling of the solvent and further processing of the dried powders, is given in Figure 2.9. A large number of novel MOF structures have been generated over the past decade via to the steps shown in Figure 9. Some examples of the MOF synthesized are MOF-2, MOF-5, IRMOF-8, and Cu-EMOF. These MOFs have already found applications in areas such as magnetism, catalysis, separations, and gas storage, placing them among the most interesting classes of solid-state materials. [54]

```
┌─────────────┐  ┌─────────────┐        ┌─────────────┐  ┌─────────────┐
│  Solution   │  │  Solution   │        │  Solution   │  │  Copper –   │
│ Formic acid,│  │  Mg-Source  │        │ Trimesic, ...│  │    metal    │
│ Acetic acid,│  │             │        │    acid     │  │  Electrode  │
└─────────────┘  └─────────────┘        └─────────────┘  └─────────────┘
        │                │                      │                │
        └────────┬───────┘                      └────────┬───────┘
                 ▼                                        ▼
┌───────────────────────────┐              ┌───────────────────────────┐
│ Precipitation, Crystallization │          │        Electrolysis         │
└───────────────────────────┘              └───────────────────────────┘
                 │               ┌──────┐                  │
                 ▼               │ Sol. │                  ▼
┌───────────────────────────┐   │Recycle│      ┌───────────────────────────┐
│      Filtration, Drying    │──│       │      │      Filtration, Drying     │
└───────────────────────────┘   └──────┘       └───────────────────────────┘
                 │                                        │
                 ▼                                        ▼
┌───────────────────────────┐              ┌───────────────────────────┐
│     Processing, Shaping    │              │     Processing, Shaping     │
└───────────────────────────┘              └───────────────────────────┘
```
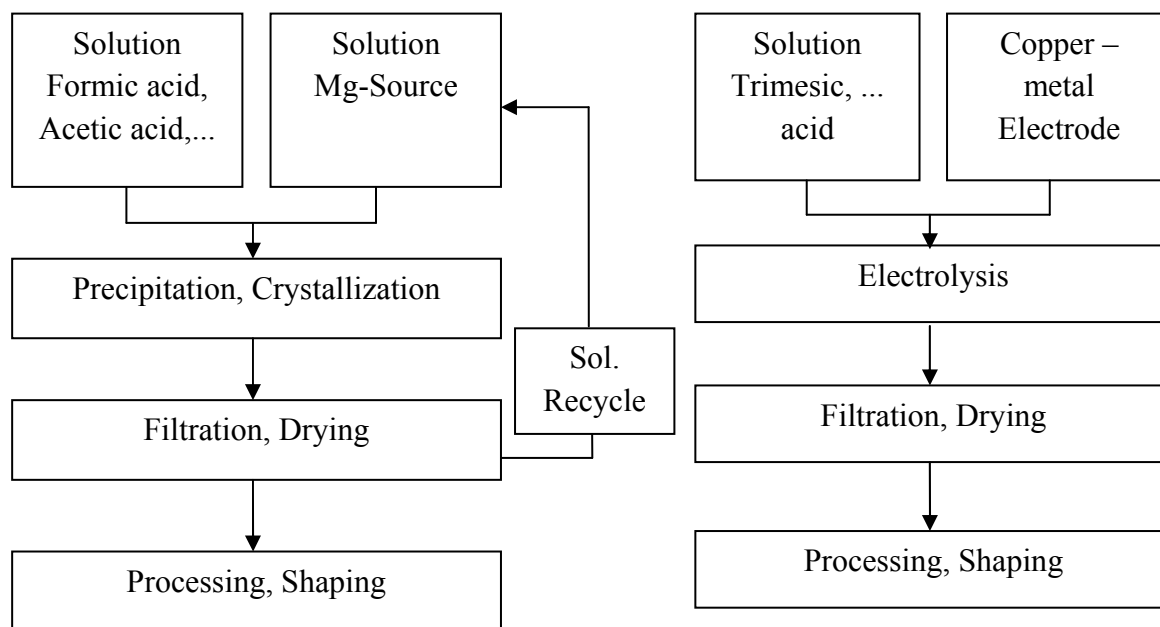
Figure 2.9 Simplified flow diagram of industrial metal-organic framework synthesis procedures via solvothermal (Mg –MOF) and electrochemical (Cu-MOF) routes, adapted from Mueller *et al.* [54]

MOF scale up studies have demonstrated that microwaves can be used to nucleate MOF crystals [55, 56]. Post-synthetic modification is a key to producing advanced MOF materials suitable for sophisticated and specialized applications. The ability to modify the physical environment of pores and cavities of MOFs, allows tuning the interaction with guest species. This modification serves as a route for tailoring the chemical reactivity and stability of the

frameworks. The potential advantages offered by post-synthetic modification are: 1) it increases the possibility to include a variety of functional groups, which would have not been possible due to MOF synthesis conditions; 2) it is easy to purify and isolate the modified product because the chemical derivatization is performed directly on the crystalline solid itself; 3) the MOF structures can be modified using different reagents, thereby generating a wide variety of topologically identical, but functionally diverse MOFs; and 4) it is possible to fine-tune and optimize the properties of MOFs by controlling the type of substituent and the degree of modification which permits multiple functional units to be introduced into a single framework in a combined manner [57].

MOFs have already found application in hydrogen storage because of their higher surface areas and chemically tunable structures [58]. Hydrogen molecules are stored in a MOF by adsorbing to its surface. Since MOFs are free of dead volume there is almost no loss of storage capacity [45]. Hydrogen binds to surfaces through strong chemical associations (chemisorption) or by weak dispersive interactions (physisorption) [59]. The latter depends on the surface area; the greater the surface area the higher the gas uptake. Thus, MOFs with higher surface area are potential candidates for hydrogen storage applications. In the case of automotive applications the temperature limits the uptake of hydrogen. But the diverse functionality of MOFs facilitates enhancing hydrogen storage by tailoring its chemical structure. In this case a MOF with a complex of platinum and activated carbon increase the storage capacity [58, 60]. Table 2.4 provides a list of MOFs that have been proposed to be most suitable for hydrogen storage.

Table 2.4 MOFs used for hydrogen storage, adapted from references [61-64].

Name of MOF	Properties
$Zn_4O(BTB)_2$, where BTB = 1,3,5-benzenetribenzoate (MOF-177)	MOF-177 with larger pore size compresses the hydrogen in the holes rather than adsorbing it on the surface. This property increases the gravimetric uptake but reduces the volumetric density when compared to MOF-5.
$Zn_4O(BDC)_3$, where BDC= 1,4-benzenedicarboxylate (MOF-5)	MOF – 5 attracted a great deal of attention from researchers and scientist due to their unique partial charges on the surface of the MOF. This provides a means to strengthen the hydrogen binding through dipole-induced intermolecular attraction. On the downside MOF-5 has inferior performance at room temperature.
$Mn_3[(Mn_4Cl)_3(BTT)_8]_2$, where BTT = benzene-1,3,5-tris(1H-tetrazole)	This MOF has increased hydrogen adsorption due to its open metal coordination site which in turn increases its performance at 298 K.
$Cu_3(BTC)_2(H_2O)_3$, where BTC = 1,3,5-benzenetricarboxylic acid	This MOF received a great deal of attention due to its paddle wheel complex from Cu^{2+} and 1,3,5 benzenetricarboxylic acid. This paddle wheel complex gives excellent control over its geometry and flexibility.

The general trend in MOFs used for gas storage is that the greater the surface area, the more gas the MOF can store in its pores, due to increased micropore volume and inherently low bulk density. In Table 2.5, the surface areas of different industrial MOFs in comparison to zeolite, activated carbon, alumina, and silica gel are presented.

Table 2.5 Surface area of different industrial MOFs and other adsorbents, adapted from *Muller* et.al [45] and others [65-67]

Materials	Langmuir surface area ($m^2 g^{-1}$)
Basolite A100 (Al-MOF)- Al-terephthalate	1100–1500
Basolite C300 (Cu-BTC-MOF) - Cu-benzene-1,3,5-tricarboxylate	1500–2100
Basolite F300 (Fe-EMOF) - Fe-benzene-1,3,5-tricarboxylate	1300–1600
Basolite Z1200 (Zn-EZIF) - Zn-2-methylimidazole	1300–1800
Basolite M050 (Mg-MOF) - Mg-formate	400–600
Zeolite	300–800
Alumina	110-470
Activated Carbon	250-950
Silica gel	400-600

Other applications of MOF include, gas purification, gas separation, and heterogeneous catalysis. The open metal site characteristics of MOF give it the ability to attract electron-rich, odor-generating molecules like alcohol, water, phospines, etc. MOF separates gas molecules according to their size or kinetic diameter. In recent studies the separation of krypton and xenon was done using MOF adsorbents. In the case of gas storage, MOFs can store carbon dioxide, carbon monoxide, methane, etc. Also, the absence of dead volume in MOF increases the volumetric storage of gas molecules compared to other adsorbents [45].

The adsorption and release of gases in the right amount is important for extending the shelf life of a product in the case of medical/food packaging. PLA is the most common biopolymer used for packaging fresh food due to its excellent barrier to flavor and aroma compounds and selective barrier properties. Because of the large variety and variable properties of fresh food/medicines, no single biobased packaging material can be said to be ideal for use with all products. In order to achieve satisfactory performance and also to utilize the extreme surface area of MOFs, PLA could be melt compounded with MOFs to create highly permeable porous patches and enhance or create a new functional membrane.

REFERENCES

REFERENCES

1. V. Siracusa, P. Rocculi, S. Romani, M.D. Rosa, "*Biodegradable polymers for food packaging: a review*", Trend in Food Science and Technology, 19, 2008, pp. 634-643.

2. M. Kolybaba, L.G. Tabil, S. Panigrahi, W.J. Crerar, T. Powell, B. Wang, "*Biodegradable Polymers: Past, Present and Future*" CSAE/ASAE Annual Intersectional Meeting, 2003.

3. J. Strnad, Z. Strnad, J. Sestak, "*Physico-chemical properties and healing capacity of potential bioactive titanium surface*", Journal of Thermal Analysis and Colorimetry, 88(3), 2007, pp.775-779.

4. A.K. Mohanty, M. Misra and L. T. Drzal, "*Natural Fibers, Biopolymers and Biocomposites*", Boca Raton, FL : Taylor & Francis/CRC Press, 2005.

5. R. A. Gross and B. Kalra, "*Biodegradable Polymers for the Environment*", Science, 297 (2), 2002, pp. 803-806

6. T.M. Aminabhavi, R.H. Balundgi, P.E. Cassidy, "*Review on biodegrable plastics*", Polymer Plastics Technology and Engineering, 29(3), 1990, pp.235-262.

7. ASTM Standards, Vol. 08.01. 1998. D883-96: Standard Terminology Relating To Plastics, New York, NY.: ASTM

8. G. Kale, R. Auras, S.P. Singh, R. Narayan, "*Biodergadability of polylactide bottles in real and simulated composting conditions*", Polymer Testing, 26, 2007, pp.1049-1061.

9. ASTM D6400-04. Standard Specification for Compostable Plastics.

10. T. Kijchavengkul, R. Auras, "Prespective: Compostabilty of Polymers", Polymer International, 57, 2008, pp. 793-804.

11. EPA, Standards for the use or disposal of sewage sludge. Environmental Protection Agency.

12. W. Amass, A. Amass and B. Tighe, "*A Review of Biodegradable Polymers: Uses, Current Developments in the Synthesis and Characterization of Biodegradable Polyesters, Blends of Biodegradable Polymers and Recent Advances in Biodegradation studies*", Polymer International, 47, 1998, pp. 89-144.

13. P. Bordes, E. Pollet, L. Averous, "*Nano-biocomposites: Biodegradable polyester/nanoclay systems*", Progress in Polymer Science, 34, 2009, pp.125-155.

14. R. A. Auras, B. Harte and S. Selke, "*Poly (Lactic Acid) Films as Food Packaging Materials*", Journal of Applied Polymer Science, 92 (3), 2004, pp. 1790 – 1803.

15. R. E. Drumright, P. R. Gruber, D. E. Henton, "*Polylactic Acid Technology*", Advanced Materials, 12 (23), 2000, pp. 1841 – 1846.

16. C. J. Webery, V. Haugaard, R. Festersen and G. Berelses, "*Production and application of biobased packaging materials for the food industry*", Food Additives and Contaminants,19, 2002, pp. 172 – 177.

17. ChemicalWeekly, May 2000, 162, pp. 24E

18. P. Gruber, Keynote Address, Massachusetts Green Chemistry Symposium, Co-Sponsored by National Environmental Technology Institute, UMASS and MA Executive Office of Environmental Affairs Toxic Use Reduction Institute, Amherst, MA, Oct.30, 2001.

19. E.T.H. Vink, D.A. Glassner, J.J. Kolstad, R.J. Wooley, R.P. O'Connor, "*The eco-profiles for current and near-future NatureWorks polylactide (PLA) production*", Industrial Biotechnology, 3(1), 2007, pp.58-81.

20. D. Garlotta, "*A literature review of poly(lactic acid)*", Journal of Polymers and the Environment, 9(2), 2001, pp. 63-84

21. R. A. Auras, B. Harte and S. Selke, "*Mechanical, physical, and barrier properties of poly(lactide) films*", Journal of plastic film and sheeting, 19(2), 2003, pp. 123-135.

22. M. Chidambarakumar "*Development of polylactic acid based blends and their nanocomposites for packaging applications*", Michigan State University, 2005.

23. S. Ramakrishna, Z.M. Huang, G. V. Kumar, A. W. Batchelor, J. Mayer, "*An introduction to Biocomposites*", Series on Biomaterials and Bioengineering – Vol. 1, Imperial College Press, 2005.

24. C.C.P.M. Verheyen, J.R. de Wijn, C.A. van Blitterswijk, K. de Groot, "*Evaluation of hydroxylapatite poly(L-lactide) composites-Mechanical behavior*", Journal of Biomedical and Material Science, 26, 1992, pp.1277.

25. Y.Z. Wan, et.al, "*In vitro degradation behavior of carbon fiber-reinforced PLA composites and influence of interfacial adhesion strength*", Journal of Applied Polymer Science, 82, 2001, pp.150

26. B.S. Kelley, R.L. Dunn, R.A. Casper, "*Totally resorbable high-strength composite material*", Polymer Science and Technology, 35, 1987, pp.75.

27. N. L. Jones, "*The Development of a Degradable Polymer Composite to be Used as a Clinical Device*", Ph.D. thesis, Vols. I-II, University of Liverpool, UK, 1996.

28. N. Ogata, et.al, "*Structure and thermal/mechanical properties of poly(L-lactide)-clay blend*", Journal of Polymer Science, 35, 1997, pp.389.

29. R. Auras, B. Harte, S. Selke, "*An Overview of Polylactides as Packaging Materials*", Macromolecular Bioscience, 4, 2004, pp. 853-864.

30. L.T. Lim, R. Auras, M. Rubino, "*Processing technologies for poly(lactic acid)*", Progress in Polymer Science, 33, 2008, pp.820-852.

31. M.S. Huda, L.T. Drzal, A.K. Mohanty, M. Mishra, "*Chopped glass and recycled newspapers as reinforcement fibers in injection molded poly(lactic acid) (PLA) composites: a comparative study*", Composite Science and Technology, 66, 2006, pp.1813-1824.

32. C. Thellen, C. Orroth, D. Frorio, D. Ziegler, J. Lucciarini, R. Farrell, "*Influence of montmorillonite layered silicate on plasticized poly(L-lactide) blown films*", Polymer, 46, 2005, pp. 11716-11727.

33. Z. Guo, L. Tan, "*Fundamentals and Applications of Nanomaterials*", Artech House, 2009.

34. BASF Chemical Company, http://www.catalysts.basf.com/Main/adsorbents/adsorbents_and_adsorption.be (March 15 2010)

35. Y. Wang, A.D. Price, F. Caruso, "*Nanoporous colloids: building blocks for a new generation of structured materials*", Journal of Materials Chemistry, 2009.

36. Brandt, R.K., M.R. Hughes, L.P. Bourget, K. Truszkowska and R.G. Greenler, "*The interpretation of CO adsorbed on Pt/SiO$_2$ of two different particle-size distributions*", Surface Science, vol. 286, pp. 15-25. 1993.

37. E.L. Cussler, "*Diffusion: Mass Transfer in Fluid Systems*", 2nd ed., pp. 308-330, 1197.

38. R.T. Yang, "*Adsorbents: Fundamentals and Applications*", John Wiley & Sons, Inc. 2003.
39. Grace chemical company http://www.grace.com/EngineeredMaterials/MaterialSciences/Zeolites/Default.aspx (March 15 2010)

40. I.E. Yuzay, R. Auras, S. Selke, "*Poly(lactic acid) and Zeolite Composites Prepared by Melt Processing: Morphological and Physical-Mechanical Properties*", Journal of Applied Polymer Science, 115 (4), 2009, pp.2262-2270.

41. K. Nakagawa, S.R. Mukai, T. Suzuki, H. Tamon, "*Gas adsorption on activated carbons from PET mixtures with a metal salt*" Carbon, 41, 2003, pp. 823-831.

42. M. Sathiyakumar, F.D. Gnanam, "*Influence of additives on density, microstructure and mechanical properties of alumina*", Journal of Materials Processing Technology, 133, 2003, pp. 282-286.

43. X. Li, Z. Li, Q. Xia, H. Xi, "*Effects of pore sizes of porous silica gels on desorption activation energy of water vapour*" Applied Thermal Engineering, 27(5-6), 2007, pp. 869-876.

44. H. Li, M. Eddaoudi, M. O'Keefe, O.M. Yaghi, "*Design and synthesis of an exceptionally stable and highly porous metal-organic framework*", Nature, 402, 1999, pp.276 -279.

45. Czaja, U. Alexander, T. Natalia, U. Mueller, "*Industrial application of metal-organic frameworks*". Chemical Society Reviews, 38(5), 2009, pp. 1284-1293.

46. The BASF chemical company, "*BASOLITE metallic organic framework data sheet*", June 2008.

47. Mueller et al. "*Metal–organic frameworks—prospective industrial applications*", Journal of Materials Chemistry, 16, 2006, 626-636.

48. S.S.Y. Chui, S.M.F Lo, J.P.H. Charmant, A.G. Orpen and I.D. Williams, "*A chemically functionalizable nanoporous material [Cu$_3$(TMA)2(H2O)3]$_n$*" Science, 283, 1999, pp.1148.

49. Xiao et al. "*High-Capacity Hydrogen and Nitric Oxide Adsorption and Storage in a Metal− Organic Framework*", Journal of the American chemical society, 129(5), 2007, pp. 1203-1209.

50. T. J. David, M.C.L. Jose, M. O'Keefe, O.M. Yaghi, "*Secondary building units, nets and bonding in the chemistry of metal-organic frameworks*". Chemical Society Review, 38 (5), 2009, pp.1257-1283.

51. D. K. Bucar, G.S. Papaefstathiou, T.D. Hamilton, Q.L. Chu, "*Template-controlled reactivity in the organic solid state by principles of coordination-driven self-assembly*", European Journal of Inorganic Chemistry, (29), 2007, pp.4559-4568.

52. E.R. Parnham, R.E. Morris, "*Ionothermal Synthesis of Zeolites, Metal-Organic Frameworks, and Inorganic-Organic Hybrids*". Accounts of Chemical Research , 40 (10), 2007, pp. 1005-1013.

53. M. Dinca, J. R. Long, "*Hydrogen storage in microporous metal-organic frameworks with exposed metal sites*", Angewandte Chemie International Edition, 47 (36), 2008, pp. 6766-6779.

54. U. Mueller, M. Schubert, F. Teich, H. Puetter, K. Schierle-Arndt, J. Pastre, "*Metal Organic Frameworks – prospective industrial applications*", Journal of Materials Chemistry, 16, 2006, pp.626-636.

55. Z. Ni, R.I. Masel, "*Rapid production of Metal-Organic Frameworks via Microwave-Assisted Solvothermal Synthesis*", Journal of American Chemical Society, 128, 2006, pp. 12394-12395.

56. J.S. Choi, W.J. Son, J. Kim, W.S. Ahn, "*Metal–organic framework MOF-5 prepared by microwave heating: Factors to be considered*", Microporous and Mesoporous Materials, 116, 2008, pp.727-731.

57. Z. Wang, S.M. Cohen, "*Postsynthetic modification of metal-organic frameworks*", Chemical Society Review, 38, 2009, 1315-1329.

58. L.J. Murray, M. Dinca, J.R. Long, "*Hydrogen Storage in Metal Organic Framework*", Chemical Scoiety Review, 38, 2009. 1294-1314.

59. D. A. McQuarrie, J. D. Simon, "*Physical Chemistry: A Molecular Approach*", Sausalito, CA: University Science Books, 1997.

60. Y. Li, R.T. Yang, "*Hydrogen Storage on Platinum Nanoparticles Doped on Superactivated Carbon*" Journal of Physical Chemistry C, 111, 2007, 11086 – 11094.

61. L. Jesse, C. Rowsell, A.R. Millward, K. S. Park, O.M. Yaghi, "*Hydrogen Sorption in Functionalized Metal-Organic Frameworks*" Journal of the American Chemical Society, 126 (18), 2004, pp. 5666-5667.

62. N.L. Rosi, J. Eckert, M. Eddaoudi, D.T. Vodak, J. Kim, M. O'Keeffe, O.M. Yaghi, "*Hydrogen Storage in Microporous Metal –Organic Frameworks*", Science, 300, 2003, pp.1127-1129.

63. M. Dinca, A, Dailly, Y. Liu, C.M. Brown, D. A. Neumann, J. R. Long, "*Hydrogen Storage in a Microporous Metal Organic Framework with Exposed Mn2+ Coordination Sites*", Journal of the American Chemical Society, 128(51), 2006, pp.16876-1883.

64. J. Y. Lee, J. Li, J. Jagiello, "*Gas sorption properties of microporous metal organic frameworks*", Journal of Solid State Chemistry, 178(8), 2005, pp.2527-2532.

65. S.M. Zemskova, J.M. Faas, C.L. Boyer, P.W. Park, J. Wen, I. Petrov, "*Study of high surface area alumina and Ga-alumina materials for denox catalyst applications*", Ceramic Engineering and Science Proceedings, 25(3), 2008, pp.299-504.

66. M.T. Beck, G. Mandy, S. Papp, I. Dekany, "*Surface modification of activated carbon and fullerene black by Dies-Alder reaction*", Colloid Polymer Science, 283, 2004, pp.237-242.

67. S.H. Kim, B.Y.H. Liu, M.R. Zachariah, "*Ultrahigh surface area nanoporous silica particles via an Aero-Sol-Gel process*", Langumir, 20, 2004, pp. 2523-2526.

CHAPTER 3. MATERIALS AND METHODS

3.1 Materials

Poly(L-lactic acid), PLA, (94% L-lactide) pellets were supplied by Natureworks LLC (Blair, NE, USA) under the trade name of Ingeo Biopolymers (PLA 4042D). The density of PLLA was 1240 kg/m^3, as reported by the company. The pellets were dried at 80°C under vacuum for at least 4 h prior to processing and then packed in air tight zipper bags.

Metallic organic framework, MOF, compounds were manufactured by BASF (Florham Park, NJ, USA) and procured from Sigma-Aldrich (St Louis, MO, USA) under the trade name of Basolite^{TM} C-300 (copper benzene-1,3,5-tricarboxylate- ($C_{18}H_6Cu_3O_{12}$)), with a surface area between 1,500 and 2,000 m^2/g, particle size distribution 15.96 μm, and bulk density of 0.35 g/cc (350 kg/m^3) (CAS No.51937-85-0). The Basolite^{TM} C300 was reactivated at 200°C for 24 h under vacuum (25 mm Hg) before processing, and then it was packed in airtight glass vials.

3.2 Equipment and Preparation:

3.2.1 Twin screw extruder

PLA was extruded in batches of 10 g. Once the PLA resin was dried and the Basolite^{TM} C-300 was activated, approximately 1, 3 and 5% wt/wt of MOF was weighed in a Discovery precision balance (OHAUS, Pine Brook, NJ, USA) and added to 10 g of PLA, mixed thoroughly, and placed in air tight glass bottles. After preparing the samples, the PLA with and without MOFs was melt compounded in a DSM Micro 15 cc extruder-compounder (DSM Research, Geleen, The Netherlands) having a vertical conical co-rotating twin screw extruding unit with screw length of 150 mm, L/D of 18 and barrel volume of 15 cc. Various kinds of samples such as

DMA bars, izod bars, tensile, flexural, and disc specimens were prepared by taking molten PLA in a preheated transfer cylinder from the extruder and then injecting them into a preheated mold that was placed in an injection molding unit using an injection pressure of about 120 psi. The optimized processing conditions for the extruder and injection molder are given in Table 3.1.

Table 3.1 Optimized parameters for extrusion in the DSM micro extruder

Variables	Extruder	Injection Molder
Temperature, °C (Top, Middle, Bottom)	190	
Screw speed, rpm	100	
Cycle time, min	5	
Melt temperature, °C	185	
Transfer cylinder temperature, °C		195
Pressure, psi		150
Mold temperature, °C		30
Residence time, sec		20

3.2.2 Metallic organic framework quantification

The amount of MOF in the 1, 3 and 5% wt/wt of the extruded composite was analyzed by determining the amount of copper in the MOF powder (control), and in the extruded composite (1, 3 and 5%). The amount of copper in the extruded composite was correlated with the amount of copper in the control to find the final percentage of MOF in the extruded composite samples. The copper content in the MOF was determined by digesting the samples by microwave by using a Microwave Drying System (Multiwave 3000, Anton Paar, Graz, Austria). A representative sample of up to 0.5 g was extracted and dissolved in 10 mL concentrated nitric acid, or alternatively, 9 mL concentrated nitric acid and 3 mL concentrated hydrochloric acid for 10 minutes in the fluorocarbon digestion vessel and heated in a microwave at high temperature and pressure. After cooling, the vessel contents were filtered, centrifuged, or allowed to settle and

then diluted to volume and analyzed by Induction Coupled Plasma – Mass Spectrophotometry (ICP-MS), ELAN DRC Plus (Perkin Elmer, Waltham, MA, USA). Tests were conducted in triplicate by the A&L Great Lakes Laboratories Inc. (Fort Wayne, IN, USA). In the ICP-MS, the samples were converted into fine aerosol droplets by a nebulizer and spray chamber system and injected into the argon plasma unit, which was then injected into the ICP. The temperature of the hot plasma was 6000 K, since most elements in the periodic table are more than 90% ionized at this temperature. The positive ions were then sent to a mass spectrometer where the ion beam is focused by electrostatic lenses and directed into the quadrupole mass filter. Here the positive ions are separated based on their mass-to-charge ratio. (The quadrupole mass filter analyzes singly charged ions from 1 to 300 amu.)

3.2.3 Film preparation

A compression molding machine Model-M, Carver Laboratory Press (Carver Inc., Wabash, IN, USA) was used to prepare films from the disc samples obtained from the microcompounder twin screw extruder. Films were compressed at 165 °C, with a residence time of 5 to 6 min, and a pressure of 5000 lb. The disc samples were placed between Teflon sheets (Small Parts Inc., FL, USA) while pressing to avoid the molten plastic sticking to the metal plates or molds.

3.2.4 Surface area of the MOF

The surface area and pore size of the MOF was analyzed using an ASAP 2010 (Micromeritics, Norcross, GA, USA) gas analyzer. An empty sample tube along with the filler rod fitted with stopper was weighed accurately using a precision balance (OHAUS, Pine Brook,

NJ, USA) with the help of a weighing support. About 0.3 to 0.5 g MOF was transferred to the sample tube along with the filler rod and stopper. The MOF in the sample tube was heated to about to 200 °C for 48 h in the degassing port of the equipment to remove any adsorbed foreign molecules. The sample tube was then transferred to the analyzing port where a controlled dose of nitrogen gas was introduced, and the gas was adsorbed or desorbed. The MOF in the sample tube was placed in a vacuum chamber at a constant temperature of -195.6 °C (liquid nitrogen), and subjected to a wide range of pressures (7 to 700 mm Hg) to generate adsorption and desorption isotherms. The amounts of gas molecules adsorbed or desorbed were determined by the pressure variations of the gas molecules by the MOF (the adsorbent). Knowing the area occupied by one adsorbate molecule, σ (for example, σ= 16.2 Å for nitrogen), and using an adsorption model, the total surface area of the material was determined. In this case, the BET (Bruner, Emmer and Teller) model [1] was used to determine the surface area of the MOF, as expressed by equation 3.1:

$$\frac{P}{n(Po-P)} = \frac{1}{cnm} + \frac{c-1}{cnm}\frac{P}{Po}$$

3.1

where P, P_o, c, n, n_m are the adsorption pressure, the saturation vapor pressure, a constant, the amount adsorbed (moles per gram of adsorbent) at the relative pressure P/P_o, and the monolayer capacity (moles of molecules needed to make a monolayer coverage on the surface of one gram of adsorbent), respectively. Through the slope and intercept of a plot of $P/[n(P_o-P)]$ against (P/P_o), n_m can be resolved. Then, the specific surface area, S, can then be derived by the equation 3.2:

$$S = NAnm\sigma$$

3.2

where, N_A is Avogadro's number. The determination of pore size and pore size distribution of the MOF can be determined from the adsorption/desorption isotherm using an assessment model, suitable for the shape and structure of the pores. In this case the pore size was determined using the isotherm from the BJH (Barret, Joyner and Halenda) equation [3]

3.2.5 Molecular Weight

The molecular weights of the PLA resin and the extruded samples (PLA and PLA with MOF (1, 3 and 5%)) were analyzed by using a gel permeation chromatograph (GPC) equipped with a Waters 1515 isocratic pump, a Waters 717 autosampler, a series of Waters Styragel columns (HR4, HR3, and HR 2), and a Waters 2414 refractive index detector interface with Water Breeze software (Waters Inc., Milford, MA, USA). Samples of 15 to 20 mg were dissolved in 10 ml of THF and heated to about 50 °C for about 2 h in order to dissolve the polymer in THF. The mixture was filtered using a 0.45 μm syringe filter, and a 100 μl sample was used to determine the molecular weight and molecular weight distribution. Polystyrene standards with molecular weight in the range of 1.31×10^3 to 3.64×10^6 Da were used for calibrating the GPC. A calibration curve was calculated by using a 3rd degree polynomial equation. The number average molecular weight (M_n), weight average molecular weight (M_w), and polydispersity index (PI) of PLA were measured. The absolute M_n and M_w were calculated by using the Mark-Houwink relation, with *a*= 0.736 and k=0.000174 (μl/s) shown in equation 3.3.

$$\eta = kM^a \qquad\qquad 3.3$$

where η=instrinic viscosity, M=molecular weight, a and k=constants

3.2.6 Contact Angle

The surface properties of the PLA and MOF were analyzed using a goniometer (Rame-Hart. Inc, Mountain Lakes, NJ, USA) by using the sessile drop method. The sample preparation methods for the PLA and MOF were as follows.

PLA: The contact angles of the PLA samples were measured in the disc samples produced from the twin screw extruder. The samples were dried at 80 ºC for 4 h. The contact angle of the PLA with water and methylene iodide was measured. At least 8 measurements on different samples were conducted for each liquid.

MOF: To measure the contact angle of the MOF, a colloidal suspension of 2% wt/vol MOF in de-ionized water was prepared. The colloid was mixed thoroughly with a magnetic stirrer for at least 5 hr at 23°C and 800 rpm. After the colloid was prepared, it was evenly distributed on a glass microscope plate (1 x 3 in^2) using a pipette. Both the pipette and the microscopic glass plate were previously cleaned with acetone and deionized water to remove impurities. Once the plates were coated with MOF, they were dried in a laminar flow for 2 d at 23 ºC. After this step, the microscopic glass plates were dried at 200 ºC for 24 hr under vacuum (25 mmHg). Glass slides were placed horizontally during the drying process. The contact angle was measured using the goniometer previously described, with water and methylene iodide. At least 8 measurements were done for each liquid.

3.2.7 Hansen's Solubility Parameters

To determine the affinity of PLA with MOF, the Hansen's solubility parameters methodology was used [4]. Specifically, the three Hansen's parameters were determined:

- δ_d, the energy from dispersion bonds

- δ_p, the energy from polar bonds

- δ_h, the energy from hydrogen bonds

These three parameters can be treated as coordinates for a point in three dimensions known as the Hansen space. The nearer two molecules are in this three-dimensional space, the more likely they are to dissolve into each other. To determine if the parameters of two molecules (usually a solvent and a polymer) are within range of solubility a value called the interaction radius (R_0) is given to the substance being dissolved. This value determines the radius of the sphere in the Hansen space, with its center is determined by the three Hansen parameters. To calculate the distance (R_a) between the Hansen parameters in Hansen space, equation 3.4 was used:

$$R_a{}^2 = 4(\delta_{d2} - \delta_{d1})^2 + (\delta_{p2} - \delta_{p1})^2 + (\delta_{h2} - \delta_{h1})^2 \qquad 3.4$$

where the subscripts 1 and 2 indicate the dispersive, polar and hydrogen bond energy of the two materials under test.

Combining Equation 3.5 with the interaction radius gives the relative energy difference (RED) of the system, which can be calculated by:

$$RED = R_a / R_o \qquad 3.5$$

A general guideline is:

RED < 1 the molecules are alike and will dissolve

RED = 1 the system will partially dissolve

RED > 1 the system will not dissolve

To determine the Hansen's Solubility Parameters for PLA and MOF, they were dissolved in a number of solvents and the mixture was subjected to 1 and 15 min sonification. After 1 and 15 min the samples were visually observed and a number on the scale of 1 to 6 was given based on the dispersion of the compound in the solvent as shown in Table 3.2

The solvents used for dissolving the PLA and MOF samples are listed in Table 3.3, with their dispersion, polar, and hydrogen bonding forces.

Table 3.2 Scoring scale for determining the Hansen's solubility parameters

Score	Comments
1	Easily dispersed, very stable dispersion
2	Takes a bit of effort to disperse, reasonably stable
3	Disperses but fairly soon starts to settle
4	Pretty reluctant to disperse
5	Some hint of dispersal
6	Just sits and laughs at the solvent

Table 3.3 Solvents used for determining the Hansen's solubility parameters

Solvent	IUPAC Name & CAS. No.	D (mJ/m^2)	P (mJ/m^2)	H (mJ/m^2)
Dichloro methane	Dichloromethane (75-09-2)	18.2	6.3	6.1
Toluene	Methylbenzene (108-88-3)	18	1.4	2
Tetra chloro ethane	1,1,2,2-Tetrachlorethane (79-34-5)	18	5	0
Methyl Ethyl Ketone	Butan-2-one (78-93-3)	16	9	5.1
Cyclohexane	Cyclohexane (110-82-7)	16.8	0	0.2
Diethylene Glycol	(2-hydroxyethoxy)ethan-2-ol (111-46-6)	16.6	12	20.7
Chloroform	Chloroform (67-66-3)	17.8	3.1	5.7
Acetone	Propanone (67-64-1)	15.5	10.4	7
THF	Oxacyclopentane (105-99-9)	16.8	5.7	8
Acetonitrile	Acetonitrile (75-05-8)	15.3	18	6.1
Dimethyl Sulfoxide	Dimethyl Sulfoxide (67-68-5)	18.4	16.4	10.2
Ethyl Acetate	Ethyl Acetate (141-78-6)	15.8	5.3	7.2
Methanol	Methanol (67-56-1)	15.1	12.3	22.3
Phenol	Hydroxybenzene (108-95-2)	17.4	4.1	13.5
DMF	*N,N*-dimethylmethanamide (68-12-2)	17.4	13.7	11.3
Hexane	Hexane (110-54-3)			
Ethanol	Ethanol (64-17-5)	15.8	8.8	19.4
Gamma Butyro Lactone	Dihydrofuran-2(3H)-one (96-48-0)	19	16.6	7.4

3.2.8 Scanning Electron Microscopy (SEM)

The morphology of the MOF powders and impact fracture surfaces of PLA and PLA/MOF composites were observed using a JOEL JSM-6400 (Joel Ltd., Tokyo, Japan) scanning electron microscope equipped with a LaB_6 gun. Before collecting the micrographs, the powders and fractured surfaces of the composites were coated with a thin layer of gold using an

Emscope SC500 sputter coater (Emscope Laboratories Ltd, Ashford, UK). Micrographs were collected from the secondary electron images obtained with a beam energy of 15 kV.

3.2.9 FTIR Spectrophotometer

The IR spectroscopic analysis of pure PLA and of PLA with 1, 3, and 5 wt% of MOF was done using an IR Prestige-21 spectrometer (Shimadzu Corporation, Tokyo, Japan). A background scan was done between wavenumbers of 4000 and 550 cm^{-1} by keeping the resolution at 4 and the number of scans at 40. After the background scan, film samples were placed in the sample holder and scanned at the same rate as the background scan. Three measurements were taken of each sample.

3.2.10 Ultraviolet/Visible Spectroscopy

The ultraviolet/visible spectroscopic analysis of the PLA and PLA/MOF film samples was obtained using a Perkin-Elmer Lambda 25 UV/Visible spectrometer (Waltham, MA, USA). A PLA blank was first placed in the UV/VIS spectrometer and scanned in the range of 190 to 800 nm. After scanning of the PLA blank, the film samples were scanned in the same range. Three measurements were obtained for each sample.

3.2.11 Colorimetry

The color of the film samples was analyzed using a Labscan XE colorimeter (Hunter Laboratories, Reston, VA, USA). The CIE L*a*b* system was used to characterize the color of the samples. The CIELAB system can be visualized as a cylindrical coordinate system in which the axis of the cylinder is the lightness variable L*, ranging from 0 to 100%, and the radii are the

48

chromaticity variables a* and b*. Variable a* changes from green (negative) to red (positive) and variable b* changes from blue (negative) to yellow (positive). Three measurements were taken of each sample. ΔE (distance between two colors) was calculated using equation 3.6:

$$\Delta E = \sqrt{\Delta L^2 + \Delta a^2 + \Delta b^2} \qquad 3.6$$

where, ΔL = L Sample - L Standard, Δa = a Sample - a Standard and Δb = b Sample - b Standard.

3.2.12 Dynamic mechanical analyzer (DMA)

A dynamic mechanical analyzer DMA Q800 (TA instruments, New Castle, DE, USA) was used to measure the thermo-mechanical properties of PLA and PLA/MOF composites. The heat deflection temperature (HDT) of the samples was measured according to ASTM D5023. The DSM molded rectangular specimens were used for the experiments. Three point bending mode was used at a controlled force of 0.25-0.28 N to measure the HDT, which was measured at 0.2% percent of strain while heating from room temperature to 100ºC under a constant load. The preload force was calculated by using equation 3.7:

$$Preload\ Force = \frac{2}{3l}\sigma t^2 w \qquad 3.7$$

where, *l* is the span length of the specimen (50 mm), σ is the stress (66 psi), t is the thickness, and *w* is the width of the specimen. At least three replicates were tested for each treatment.

The loss modulus, storage modulus and tan delta were measured according to the ASTM D4065 standard using the dual cantilever mode at an amplitude of 15μm and frequency of 1 Hz. The specimens were heated from 0 to 100 °C at the rate of 5 °C/min under the DMA-multi-

frequency strain. The glass transition temperature was determined from the storage modulus, loss modulus and tan delta. At least three replicates were tested for each treatment.

3.2.13 Izod Impact Tester

A monitor Izod impact tester TMI 43-02-01 (Testing Machines Inc., Ronkonkoma, NY, USA) was used with a l-1b pendulum to measure the notched izod impact strength of samples at ambient conditions according to the ASTM D256 standard. A TMI notching cutter (model – 22-05) was used to notch the samples as per the standard. At least five specimens were tested for each treatment.

3.2.14 Tensile test

A universal testing machine UTS SFM – 20 (United Calibration Corporation, Huntington Beach, CA, USA) was used to measure the tensile properties of the PLA and PLA/MOF samples (i.e., % elongation at break, % elongation at strain, tensile strength, and the modulus of elasticity.) The tensile testing was done as per ASTM D638 standard except the sample size and the gauge length, since the DSM micro-extruder produces samples that are smaller in size than the standard ASTM samples. Therefore, a gauge length of 1 in was followed instead of the standard 2 in gauge length. At least five specimens were tested for each sample and a load cell of 1000 lb was used for the experiments.

3.2.15 Differential scanning calorimetry (DSC)

The thermal properties of PLA and PLA/MOF composites extruded samples and films were studied by using a differential scanning calorimeter, DSC Q200 (TA Instruments, New

Castle, DE). A heat-cool-heat cycle was used to measure the glass transition temperature (T_g), onset of cold crystallization temperature (T_{cc} onset), T_{cc}, onset of melting temperature (T_m onset) and T_m of the samples. Samples of 7 to 10 mg were non-hermetically sealed in an aluminum pan. After placing the sample and the reference in the DSC cell, the cell was heated from room temperature to 200°C at 10°C/min. After the completion of the first heating cycle, the cell was cooled from 200 to 0°C at 10°C/min, and for the second heating cycle the same ramping conditions were used as that of the first heating cycle. T_{cc} onset and T_{cc} are reported from the first heating run, and T_g, T_m onset and T_m were obtained from the second heating run. The percent crystallinity of the extruded samples from DSM was calculated using equation 3.8:

$$X_c(wt.\%) = 100 * \frac{\Delta H_m - |\Delta H_c|}{\Delta H_f (1-x)} \qquad\qquad 3.8$$

ΔH_m = enthalpy of melting, ΔH_c = enthalpy of cold crystallization, ΔH_f = enthalpy of fusion of 100% crystalline PLA, which is 93.7 J-g^{-1}, and x is the weight fraction of MOF in the composite. At least three specimens were tested for each composite combination.

3.2.16 Barrier properties

The Barrier properties of the films were measured using the film samples produced in the compression molding machine. The water vapor transmission rate (WVTR) was determined using a Permatran W3/31 (MOCON Inc, Minneapolis, MN, USA). The conditions used for the experiment were as follows: area of the film 3.14 cm^2; RH: 100%; carrier gas N$_2$; temperature 23°C. The WVTR values were used to calculate the water vapor permeability from equation 3.9:

$$Water\,vapor\,permeability = \frac{Water\,vapor\,transmission\,rate(q)*thickness(l)}{partial\,pressure(\Delta p)*time(s)*area(m^2)} \qquad 3.9$$

The oxygen transmission rate (O_2TR) was determined with an Oxtran 100 –Twin (MOCON Inc., Minneapolis, MN, USA). The conditions used for the experiment were as follows: area of the film 3.14 cm^2; permeant = 0.21 atm of O_2; carrier gas, N_2 containing 2% H_2; temperature 23°C; and 0% relative humidity. The OTR values were used to calculate the oxygen permeability by using equation 3.10:

$$Oxygen\,permeability = \frac{Oxygen\,transmission\,rate(q)*thickness(l)}{partial\,pressure(\Delta p)*time(s)*area(m^2)} \qquad 3.10$$

3.2.17 Isotherm

The moisture sorption and desorption of the MOF, PLA and PLA/MOF composite of the compression-molded film was examined by gravimetric analysis using a SGA-100 from VTI Corporation (Florida, USA). The films (5-10 mg) were exposed to relative humidity of 10, 30, 40, 50, 60, 70, and 90% at 23ºC and the sorption and desoprtion isotherms of the films were plotted.

3.2.18 Statistical analysis

At least two runs (i.e. extrusion using twin screw extruder) for each treatment (i.e. 1, 3, 5 % wt/wt) were conducted for each property. If needed, a third run was conducted for further analysis. Repeated measure analysis of variance (ANOVA) and Tukey tests were used to test the significant differences between the treatment and control means.

REFERENCES

REFERENCES

1. S. Brunauer, P.H. Emmett, E. Teller, "*Adsorption of gases in multimolecular layers*". Journal of the American Chemical Society. 1938, 60, pp. 309–319.

2. J.C.Groen, L.A.A. Peffer, J.P.Ramirez, "*Pore size determination in modified micro- and mesoporous materials. Pitfalls and limitations in gas adsorption data analysis*", Microporous and Mesoporous Materials, 60, 2003, pp. 1-17.

3. E.P. Barrett, L.G. Joyner and P.P. Halenda, "*The Determination of Pore Volume and Area Distributions in Porous Substances. I. Computations from Nitrogen Isotherms*", Journal of American Chemical Society, 73, 1951, pp. 373-380.

4. R. Auras, B. Harte, S. Selke, "*Sorption of ethyl acetate and d-limonene in poly(lactide) polymers*", Journal of the science of food and agriculture, 86, 2006, pp. 648-656.

CHAPTER 4. RESULTS AND DISCUSSION

4.1 DSM samples

Disc, rectangular and dumb-bell shaped samples were produced using the micro-extruder.

Disc samples were used for measuring optical, physical and barrier properties. Rectangular

samples were used for measuring thermo-mechanical properties and Izod impact strength. The

tensile strength of the samples was analyzed by using the dumb-bell shaped samples. The

samples produced from the micro-extruder are shown in Figure 4.1.
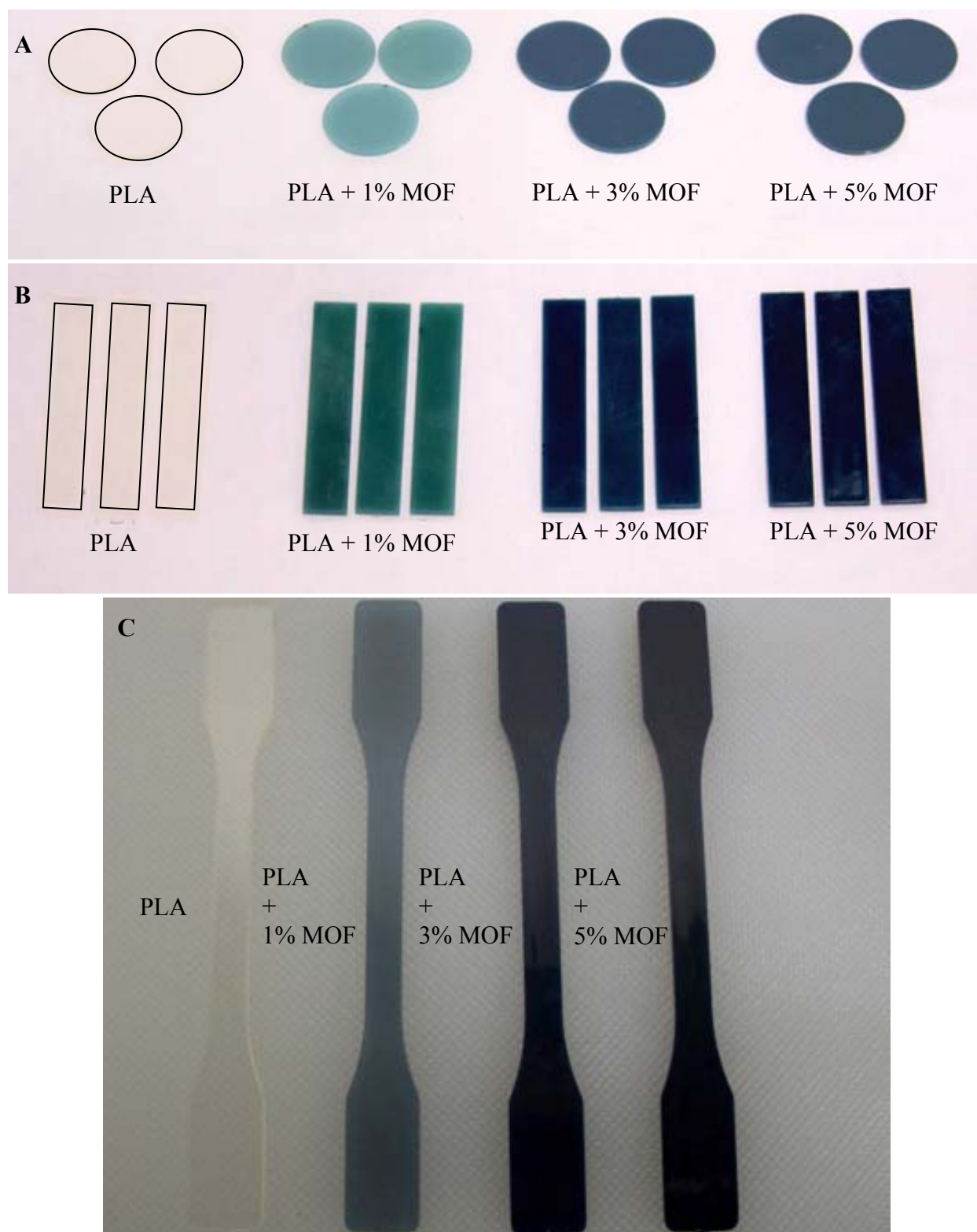
Figure 4.1 DSM specimens (A) disc; (B) rectangular; and (C) dumb-bell samples. ("For interpretation of the references to color in this and all other figures, the reader is referred to the electronic version of this thesis.")

4.2 Compression molding

Compression molded films were used for analyzing thermal, optical and barrier

properties. The PLA and PLA/MOF composite films (1, 3 and 5% wt/wt) produced by

compression molding are shown in Figure 4.2.
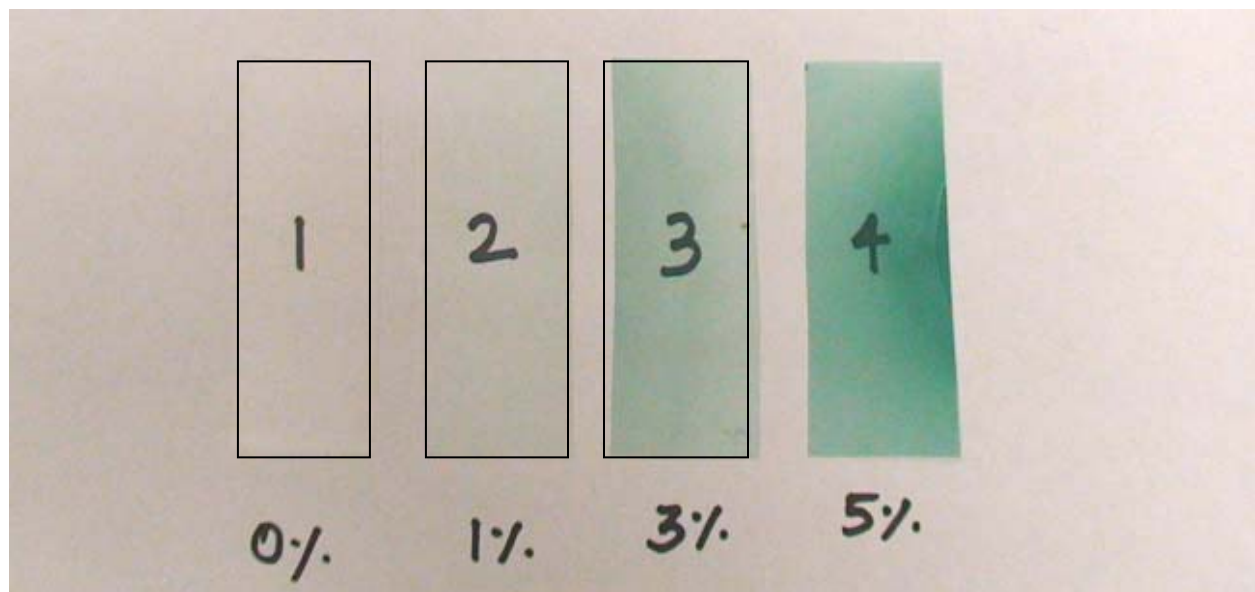
Figure 4.2 Compression molded film samples: (1) PLA, (2) PLA + 1%MOF, (3) PLA + 3% MOF, and (4) PLA + 5%MOF ("For interpretation of the references to color in this and all other figures, the reader is referred to the electronic version of this thesis.")

4.3 Quantification of MOF

The actual amount of MOF in the 1, 3 and 5% wt/wt of the extruded composite samples was determined by ICP-MS, and the values are shown in Table 4.1. The MOF % was calculated by dividing the copper content in the extruded composite with the value of the copper content from the pure MOF (control). MOF content in the extruded composite was lower than the actual MOF % that was added to the PLA while preparing the samples. This loss could occur due to MOF loss during transferring from the weighing pan to the bottle filled with PLA and also during loading of the samples into the DSM Micro Extruder. The MOF powders are highly electrostatic, so they tend to get stuck in the weight pan, bottle and feeder of the extruder. The same observation was reported by Hilal during the quantification of zeolite in polypropylene composite films. In the case of 4% wt/wt loading of zeolite in polypropylene films the amount quantified by TGA was about 2%.[1] In case of PLA/MOF, much lower losses were found in the extruded samples.

Table 4.1 Quantification of MOF content in the extruded samples

Material	Introduced wt. (%)	Copper Content (mg/kg)	MOF wt. (%)	Average wt. (%)
MOF	Control	260075	Control	Control
1%MOF	0.99	1659.9	0.64	0.59±0.07
	0.99	1329.6	0.51	
	0.99	1639.7	0.63	
3%MOF	2.91	5594.7	2.15	2.08±0.07
	2.91	5343.4	2.05	
	2.91	5252.7	2.02	
5%MOF	4.76	11589	4.46	4.41±0.12
	4.76	11091.6	4.26	
	4.76	11697.2	4.50	

Although the actual final concentration of the MOF in samples was lower than the introduced, the samples will still be indentified in this thesis as PLA, PLA plus 1, 3, and 5% MOF for simplicity. The reader should note that the actual values of MOF in the samples are the indicated in Table 4.1.

4.4 Contact Angle

Contact angle measurement indicates the angle at which the liquid/vapor interface meets the solid surface. It is based on the thermodynamic equilibrium between three phases (i) liquid (ii) solid and (iii) vapor phase. Young's relationship forms the basis to determine the equilibrium contact angle. Young's equation assumes a perfectly flat surface, and it does not addresses surface roughness and impurities, which might cause a deviation in the contact angle. Based on Young's equation many theories and equations have been developed, including Fowkes, geometric mean, Wu harmonic mean, acid-base, and the equation of state. Table 4.2 shows these equation and their terminology.

Table 4.2 Main theories and equation of contact angle (Young, Geometric mean, Wu-harmonic mean, Acid-base, Equation of state)

Theory	Mathematical representation
Young	$\gamma_L \cos\theta = \gamma_S - \gamma_{SL}$
Fowkes	$\gamma_L(1+\cos\theta) = 2\sqrt{\gamma_S^d \gamma_L^d}$
Geometric mean	$\gamma_L(1+\cos\theta) = 2\sqrt{\gamma_S^d \gamma_L^d} + 2\sqrt{\gamma_S^p \gamma_L^p}$
Wu-harmonic mean	$\gamma_L(1+\cos\theta) = 4\dfrac{\gamma_S^d \gamma_L^d}{\gamma_S^d + \gamma_L^d} + 4\dfrac{\gamma_S^p \gamma_L^p}{\gamma_S^p + \gamma_L^p}$
Acid-base	$\gamma_L(1+\cos\theta) = 2\sqrt{\gamma_S^{LW} \gamma_L^{LW}} + 2\sqrt{\gamma_S^+ \gamma_L^-} + 2\sqrt{\gamma_S^- \gamma_L^+}$
Equation of state	$\gamma_L(1+\cos\theta) = 2\sqrt{\gamma_S \gamma_L}\left[1 - \beta_1(\gamma_S - \gamma_L)^2\right]$

γ_L = Surface tension of liquid, γ_S = Surface tension of solid, γ_{SL} = Surface tension of liquid-solid, γ_S^d = Dispersive surface tension of solid, γ_L^d = Dispersive surface tension of liquid, γ_S^p = Polar surface tension of solid, γ_L^p = Polar surface tension of liquid, γ_S^{LW} = Lifshitz- van der Waals (LW) component of surface tension of solid, γ_L^{LW} = Lifshitz- van der Waals (LW) component of surface tension of liquid, γ_S^+ = Electron acceptor parameter of solid, γ_L^- = Electron donor parameter of liquid, γ_S^- = Electron donor parameter of solid, γ_L^+ = Electron acceptor parameter of liquid, β_1 = constant, and θ = Contact angle.

Initially, the contact angle of the PLA and MOF was measured using water (polar) and diiodomethane (non-polar). The Wu harmonic and geometric mean theory was used to calculate the surface energy of PLA and MOF for assessing their blending capability. The contact angle determined by using water and diiodomethane combination could not be used to calculate the

surface energy of the PLA and MOF due to its large variation between the PLA and MOF. In order to overcome this limitation, several polar (ethylene glycol, formamide) and non-polar (hexane, octane) liquids were used to estimate the surface energy. The surface tensions, dispersive and polar components of various solvents are given in Table 4.3. The sessile drop images of the PLA and MOF with various solvents are shown in Figures 4.3 and 4.4. Ethylene glycol and diiodomethane (methylene oxide) combination were used to estimate the surface energy of PLA and MOF. The contact angle, surface energy, polarity and work adhesion parameters of the PLA and MOF determined by using the Wu-harmonic mean and Geometric mean method are shown in Table 4.4. The interfacial tension and spreading coefficient are shown in Table 4.5.

Table 4.3 Surface tension, dispersive and polar component of test liquids

Liquid	Surface Tension $(mJ.m^{-2})$	Dispersive Component $(mJ.m^{-2})$	Polar Component $(mJ.m^{-2})$
Hexane	18.4	0	0
Water	72.8	25.5	25.5
Formamide	58.0	2.28	3.96
Diiodomethane	50.8	0	0
Ethylene Glycol	47.7	26.4	21.3

Table 4.4 Contact angle and surface energy parameters of PLA and MOF

Mat.	Ethylene Glycol		Methylene Iodide		Surface energy mJm^{-2}			Polarity	Work Adhesion mJm^{-2}
	Harmonic Mean Method								
	θ	Cos θ	θ	Cos θ	Polar	Dispersive	Total		
PLA	57.1±3.3	0.5±0.1	37.6±3.3	0.8±0.0	3.1±1.2	39.2±2.9	42.2±2.0	0.1±0.0	62.1±3.2
MOF	53.3±2.5	0.6 ±0.0	45.4±4.3	0.7±0.1	6.0±1.3	31.8±2.9	37.8±1.9	0.2±0.0	
	Geometric Mean Method								
	θ	Cosθ	θ	Cosθ	Polar	Dispersive	Total		
PLA	57.1±3.3	0.5±0.1	37.6±3.3	0.8±0.0	0.7±0.5	45.2±2.3	45.9±1.9	0.02±0.0	82.2±4.3
MOF	53.3±2.5	0.6 ±0.0	45.4±4.3	0.7±0.1	1.7±0.9	39.5±3.3	41.2±2.5	0.04±0.0	

Table 4.5 Interfacial tension and spreading coefficient of PLA and MOF

Method	Surface energy mJ.m^{-2}		Work adhesion mJ.m^{-2}	Interfacial Tension mJ.m^{-2}	Spreding Coefficient mJ.m^{-2}
	PLA	MOF			
Geometric Mean	45.9±1.9	41.2±2.5	82.2±4.3	16.3±4.3	13.2±4.3
Harmonic Mean	42.2±2.0	37.8±1.9	62.1±3.2	36.4±6.3	33.3±6.3

The contact angle of PLA with diiodomethane coincides well with the work done by Schwach *et.al.* [7] The MOF contact angles were not found reported in the literature. The MOF particles can be tailored with either hydrophobic or hydrophilic properties, and have good ion exchange properties higher than zeolites. [8, 9] The contact of angle of silica has been reported. [9, 10] The contact angle of porous materials increases as their polarity of the organic group decreases. It was reported that the contact angle of carboxyl-, hydroxyl-, vinyl- and methyl- terminated alkylsilane on silica were 32, 48, 97 and 108°. For MOF, the measured contact angle with water was found to be 145° which is higher than that of 114° reported for Organo TricholoroSilane (OTS) -silylated silica surface [12] and lower when compared to that of 163° reported for C18- zeolite with OTS. However, contact angle of particles with higher surface areas such as zeolites, silica, and MOF need to be interpreted with caution, due to surface roughness, deformation of particles and particle porosity. [13, 14]

The interfacial tension and the work adhesion parameter value derived through the Wu harmonic and geometric mean can be used to assess the compatibility of two materials. The greater the theoretical work adhesion and lower the interfacial tension, the more compatible the materials are. According to Table 4.3, the greater theoretical work

adhesion parameter of PLA and MOF may indicate that the PLA and MOF composite will have good compatibility. Also, the positive spreading coefficient indicates that MOF may disperse in PLA. In the case of mixed matrix membranes (MMMs), the affinity between the two phases is an important factor. The compatibility between inorganic filler and amorphous rubbery polymer was good due to the greater mobility of polymer chains when compared to amorphous glassy polymers. [15 – 17] But, amorphous glassy polymers are widely used in gas separation due to their greater transport characteristics. The dispersion of inorganic fillers into the matrix of glassy polymers cause defects at the interface due to the rigidity of the polymer chains. The addition of zeolite to the polymer matrix increased the permselectivity and decreased the permeability due to blockage of pores by the polymers. [18] The affinity of the MOF with polymer matrices is not yet reported in the research literature, but the contact angle studies revealed that MOF may disperse into the PLA matrix.
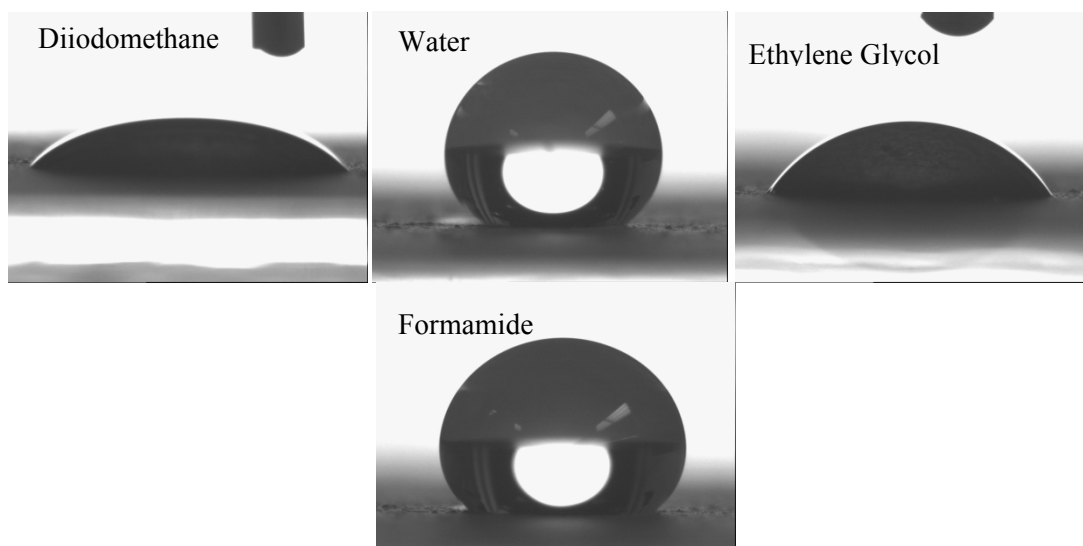
Figure 4.3 Sessile drop images of MOF on diiodomethane, water, ethylene glycol and formamide
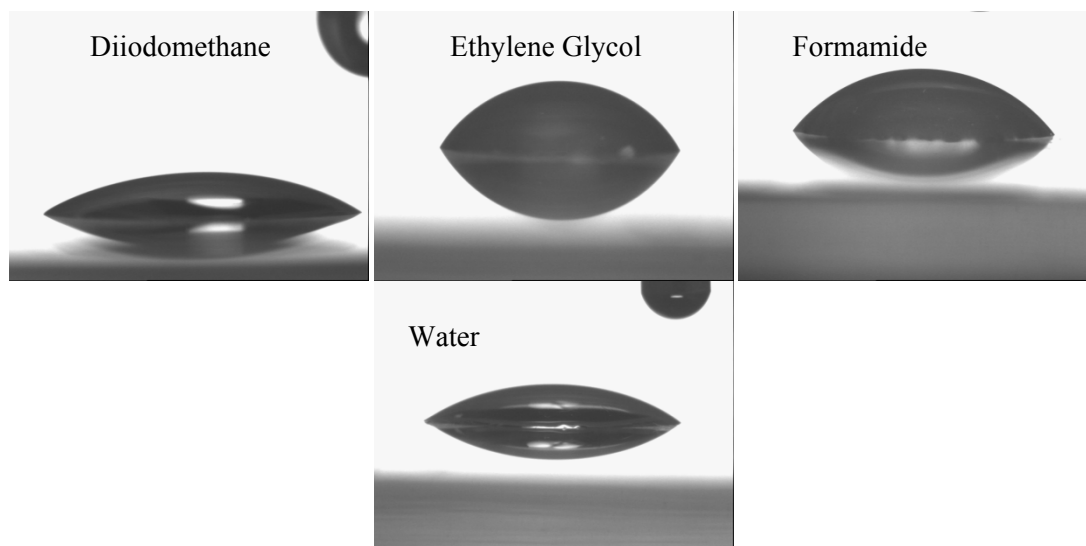
Figure 4.4 Sessile drop images of PLA on diiodomethane, ethylene glycol, formamide, and water.

4.5 Solubility parameters

Solubility parameters were determined according to the Hansen's solubility parameter methodology. The solubility scoring numbers according to the methodology explained in the section 3.2 for the PLA and MOF when dissolved in serious of solvents are given in Table 4.6.

Table 4.6 Scoring of PLA and MOF in various solvents, according to the scoring scale defined in Table 3.3

IUPAC Name & CAS. No.	Solvent	Assigned Numbers	
		MOF	PLA
Dichloromethane (75-09-2)	Dichloro Methane	3	2
Methylbenzene (108-88-3)	Toluene	3	6
1,1,2,2-Tetrachlorethane (79-34-5)	Tetra Chloro Ethane	3	2
Butan-2-one (78-93-3)	Methyl Ethyl Ketone	6	6
Cyclohexane (110-82-7)	Cyclo Hexane	6	6
(2-hydroxyethoxy)ethan-2-ol (111-46-6)	Diethylene Glycol	5	6
Chloroform (67-66-3)	Chloroform	5	2
Propanone (67-64-1)	Acetone	3	6
Oxacyclopentane (105-99-9)	THF	3	2
Acetonitrile (75-05-8)	Acetonitrile	3	6
Dimethyl Sulfoxide (67-68-5)	Dimethyl Sulfoxide	3	6
Ethyl Acetate (141-78-6)	Ethyl Acetate	3	5
Methanol (67-56-1)	Methanol	3	6
Hydroxybenzene (108-95-2)	Benzanol	3	6
N,N-dimethylmethanamide (68-12-2)	DMF	3	6
Hexane (110-54-3)	Hexane	4	6
Ethanol (64-17-5)	Ethanol	6	6
Dihydrofuran-2(3H)-one (96-48-0)	Gamma Butryo Lactone	3	6

PLA dissolved completely in THF, tetrachloroethane, dichloromethane and chloroform. Figure 4.5 shows PLA in these solvents, as completely dissolved in these

solvents. In the other solvents, PLA did not dissolve settled to the bottom without any

visual flurries, swelling or reaction with the solvent.
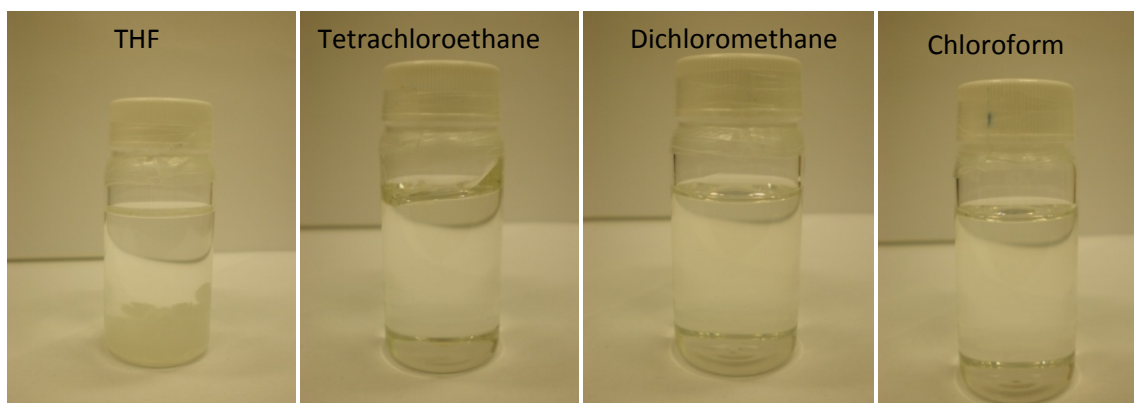
Figure 4.5 Dissolution of PLA in THF, tetrachloroethane, dichloromethane, and chloroform ("For interpretation of the references to color in this and all other figures, the reader is referred to the electronic version of this thesis.")

MOF powder did not completely dissolve in any of the solvents used for

measuring the solubility parameters. Instead it was dispersed when the solvent was added

to it, and after sonication started to settle down. The settling time varied according to the

density of the solvent, the higher the density the more time the MOF took to settle down.

Figure 4.6 indicates how the MOF was dispersed in various solvents after 15 min of

sonication. In some solvents the MOF settled down completely, and in others it started to

settle down after 15 min sonication.
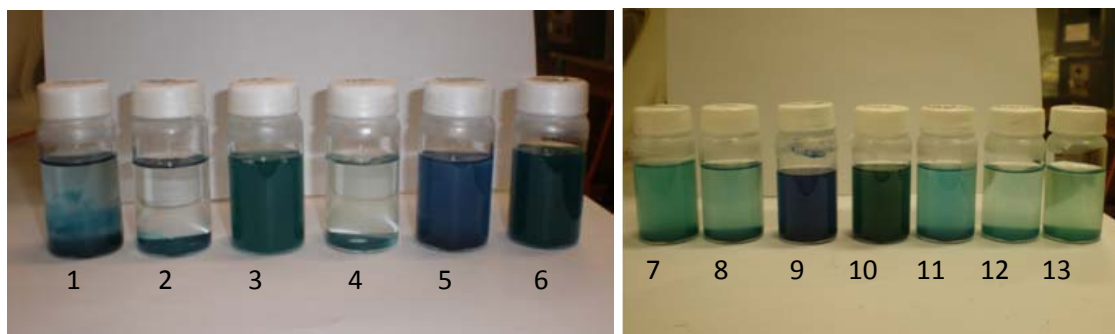
Figure 4.6 Dispersion of MOF particles in various solvents (1- Dichloro Methane, 2- Tetra chloro ethane, 3- Toluene, 4- Cyclo Hexane, 5- Diethylene Glycol , 6- Methyl Ethyl ketone, 7- Methanol, 8- THF, 9-Chloroform, 10- Dimethyl Sulfoxide, 11- Ethyl Acetate, 12- Acetone, 13- Acetonitrile) ("For interpretation of the references to color in this and all other figures, the reader is referred to the electronic version of this thesis.")

After two days of storage, the MOF in all the liquids settled down completely as shown in Figure 4.7
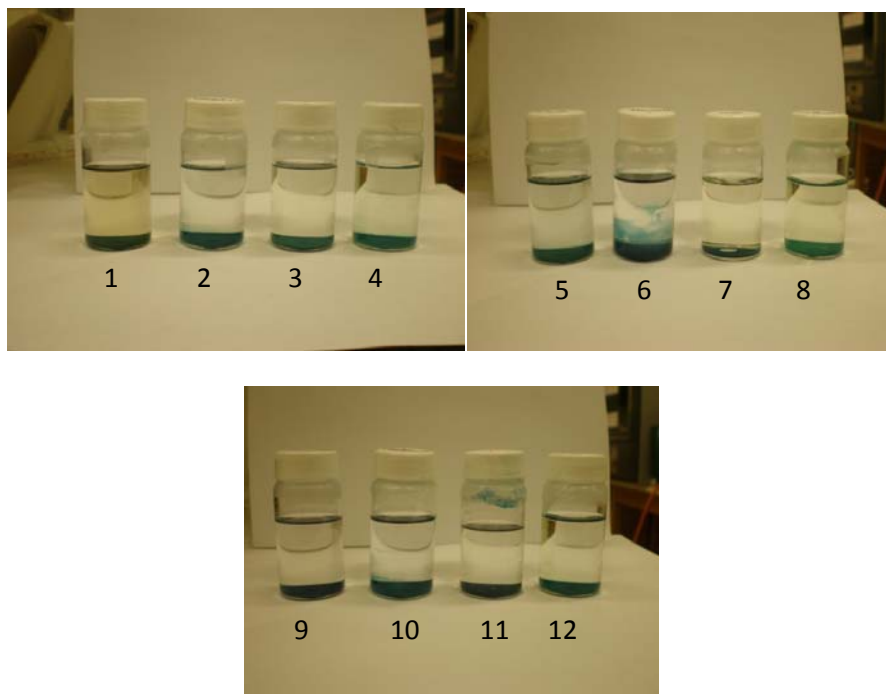
Figure 4.7 MOF particles in various solvents after 2 days of storage (1- Dimethyl Sulfoxide, 2- Ethyl Acetate, 3- Tetrachloro ethane, 4- Methanol, 5- Diethylene Glycol , 6- Toluene, 7- Methyl Ethyl ketone, 8- Acetonitrile, 9- Dichloro Methane, 10- Cyclo Hexane, 11- Chloroform, 12- THF) ("For interpretation of the references to color in this and all other figures, the reader is referred to the electronic version of this thesis.")

68

HSPiP® software (Horsholm, Denmark) was used to calculate the Hansen solubity parameters using the data from Table 4.6 obtained by dispersing the PLA and MOF in the mentioned solvents. Each solvent has unique polar, dispersion and hydrogen forces as reported in Table 3.2. The dispersion, polar, hydrogen forces and interaction radius as calculated from the HSPiP® software are shown in Table 4.7.

Table 4.7 Dispersion, polar, and hydrogen parameters for PLA and MOF

Material	Dispersion δ_D (MPa$^{1/2}$)	Polar P δ_P(MPa$^{1/2}$)	Hydrogen Force δ_H (MPa$^{1/2}$)	Interaction Radius R
PLA	17.63	5.86	6.36	2.9
MOF	17.92	9.9	10.68	3.9

The modified difference between the HSP for the MOF and PLA (R_a) was calculated using equation 4.1

$$(R_a)^2 = 4(\delta_{D2} - \delta_{D1})^2 + (\delta_{P2} - \delta_{P1})^2 + (\delta_{H2} - \delta_{H1})^2 \qquad 4.1$$

Based on the δ_D, δ_P, δ_H, obtained from the HSPiP® software, the R_a was found to be 5.94 for the PLA and MOF. The Relative Energy Difference (RED = R_a/R_o) can be used to assess the affinity of the two materials in terms of its solubility. A RED number of 0 is found for no energy difference. RED number less than 1 indicates high affinity, RED equal to or close to 1 is the boundary condition, and progressively higher RED numbers indicates lower affinity between two materials. The calculated RED of the PLA and MOF is 1.5. This indicates poor affinity between PLA and MOF. This is different from the results predicted from the contact angle measurements, which assessed the PLA and MOF to be compatible. [19]

4.6 Molecular weight

Weight average molecular weight (M_w), number average molecular weight (M_n), and molecular weight distribution (PDI) of PLA resin and PLA with and without MOF were determined by GPC and are shown in Table 4.8. PLA degrades when exposed to high temperature and humidity. The reduction of M_n of the extruded samples when compared to the pure PLA resin can be attributed to the thermal degradation of the PLA during extrusion due to the presence of residual moisture in the resin after drying. These factors cause chain scission and consequently decrease the molecular weight and the chain length. It was reported that amorphous PLA reduced its M_w when exposed to 60ºC and 80% RH for less than a month [20]. The addition of MOF during melt compounding of PLA did not significantly change the M_w, M_n, and PDI of the PLA, significantly. This confirms that the addition of MOF does not have a detrimental effect on the chain length of the PLA. Sinha Ray et.al. and Yuzay et.al. reported that the incorporation of montmorillonite and zeolite to PLA resulted in a reduction of M_n and M_w of the PLA matrix of up to 12 and 14%, respectively. [3]

Table 4.8 Number average molecular weight (M_n), weight average molecular weight (M_w), and molecular weight distribution (PDI) of PLA resin and PLA/MOF composites

Samples	M_n(kDa)	M_w(kDa)	PDI
PLA Resin	87.1±1.04[a]	123.81±0.86[a]	1.42±0.01[a]
PLA	82.09±0.65[b]	120.79±0.23[a]	1.47±0.01[a]
PLA+1%MOF	83.91±1.92[b]	123.76±3.68[a]	1.45±0.03[a]
PLA+3%MOF	81.89±1.01[b]	119.97±1.01[a]	1.47±0.02[a]
PLA+5%MOF	81.71±1.15[b]	119.39±0.51[a]	1.46±0.02[a]

Note: Values are represented as averages ± standard deviation. Values with different superscript letters in the same column are significantly different at α = 0.05 (Tukey – HSD)

4.7 Surface Area

The surface area, pore volume, and the pore diameter as reported by the ASAP 2010 is tabulated in Table 4-9. The surface area coincided with the specification from Sigma Aldrich (1400 – 2100 m^2/g). The change in surface area between the two runs could be due to the MOF being from different batches as well as experimental uncertainty. The pore diameter was not reported by the supplier, and it was found to be in the range of 1.86 to 3.54 nm as determined by the BET and the BJH methods, respectively. The nitrogen adsorption and desorption isotherm are shown in Figure 4-8 and 4-9. The adsorption and desorption isotherms were used to calculate the surface area and pore size distribution of the porous materials. The amount of gas adsorbed is expressed as a function of the equilibrium relative pressure, P/P_O. The data from the

nitrogen adsorption isotherm can be plugged into equations 3.1, 3.2 and 3.3 to calculate

the surface area and pore size distribution of the MOF particles. [21]

Table 4.9 BET surface area, micropore volume, and pore diameter of MOF

RUN	BET surface area (m^2/g)	Micropore Volume (cm^3/g)	Pore Diameter by BET (nm)	Pore Diameter by BJH (nm)
1	1683.94 ± 37.76	0.634	1.86	3.54
2	1449.79 ± 33.46	0.549	1.89	3.66

Figure 4.8 Nitrogen adsorption isotherm ("For interpretation of the references to color in this and all other figures, the reader is referred to the electronic version of this thesis.")

72

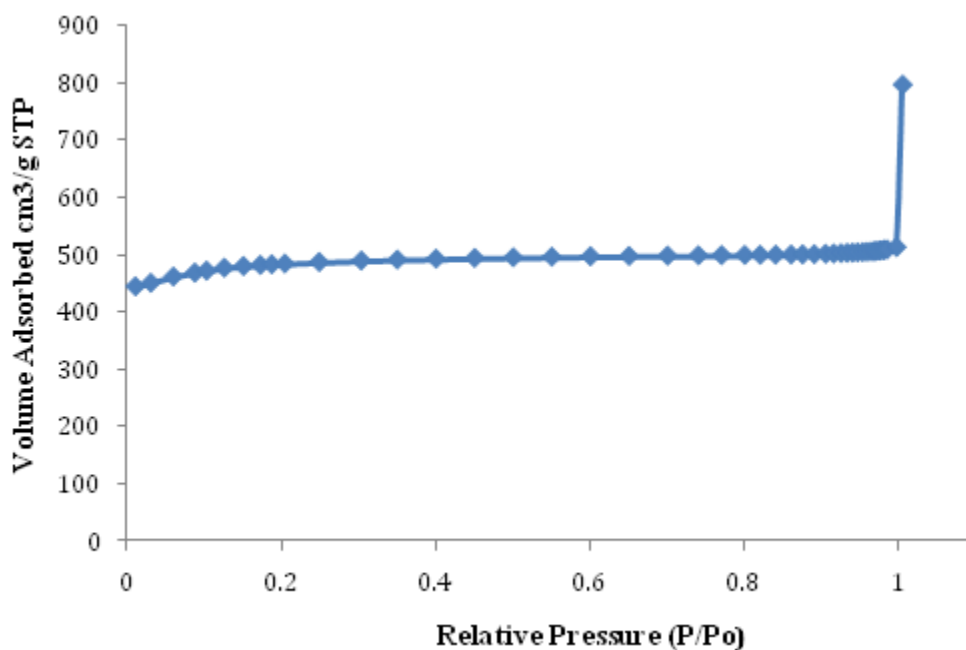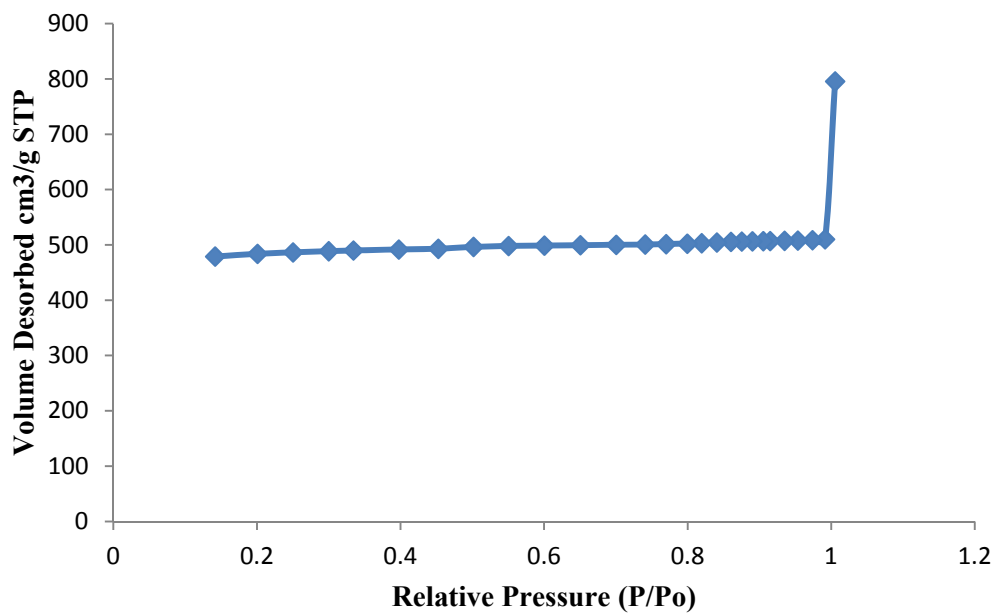**Figure 4.9** Nitrogen desorption isotherm ("For interpretation of the references to color in this and all other figures, the reader is referred to the electronic version of this thesis.")

4.8 Scanning Electron Microscopy (SEM)

Figure 4.10 shows a microscopic image of the geometry of MOF powders, which are irregular polyhedra in shape and range from 5-20 μm in size.
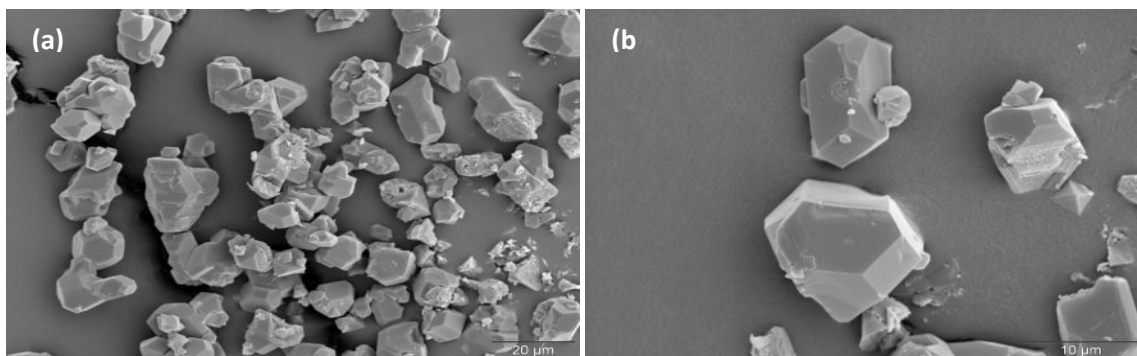
Figure 4.10 SEM images of MOF powders. a) Magnification: 1000X, scale bar: 20 μm, b) Magnification: 3000X, scale bar: 10 μm (Images were obtained and provided by Yuzay, I.)

Figure 4.11 displays the SEM images of PLA and PLA/MOF composites. Figure 4.11 (a) exhibited a typical brittle fracture of the PLA specimen and the fracture surface appeared to be very smooth. After inclusion of MOF, a ductile fracture surface became characteristic in all the micrographs (Figure 4.11 (c-i)).

The composite samples produced using 2 min mixing time in the mini-extruder exhibited a non-uniform distribution of MOF. The MOF powders tend to agglomerate in the PLA matrix (Figure 4.11 (c-d)). A better dispersion of MOF powders within the PLA samples was observed when a mixing time of 5 min was used (Figure 4.11 (e-i)). The images taken at high magnification levels revealed void formation at the interface of the PLA matrix and the MOF (Figure 4.11 (h-i)). The formation of voids shows poor interfacial adhesion between the PLA matrix and the MOF powders, which was opposite to the contact angle predictions.
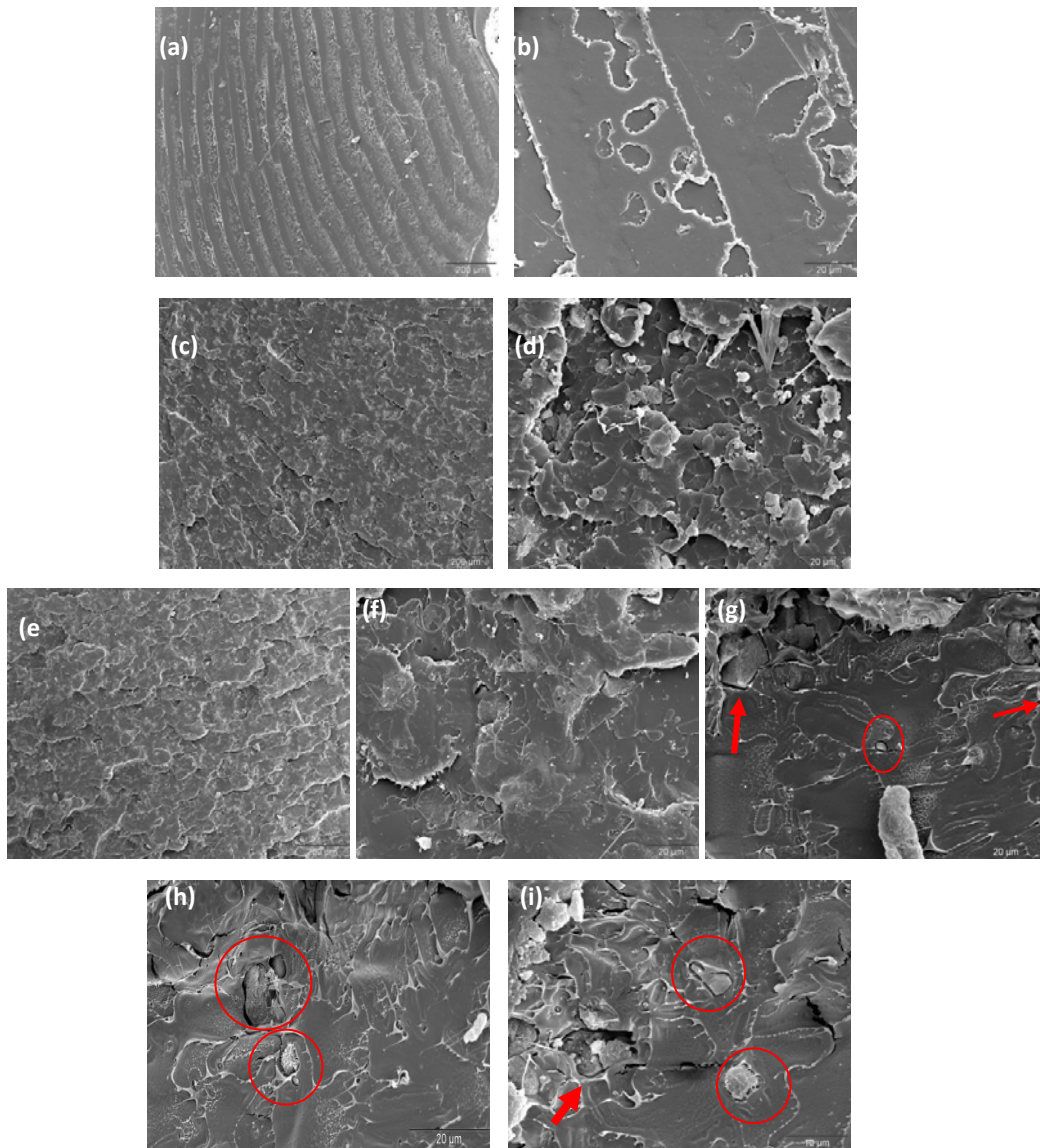
Figure 4.11 SEM images of PLA and PLA composites with 5 wt% MOF fabricated using 2 and 5 min mixing time in the micro-compounder (Images were obtained and provided by Yuzay, I.)

a) PLA magnification: 100X, scale bar: 200 μm, **b)** PLA magnification: 1000X, scale bar: 20 μm **c)** PLA/MOF 5wt%, 2 min mixing time, magnification: 100X, scale bar: 200 μm **d)** PLA/MOF 5wt%, 2 min mixing time, magnification: 1000X, scale bar: 20 μm **e)** PLA/MOF 5wt%, 5 min mixing time, magnification: 100X, scale bar: 200 μm **f)** PLA/MOF 5wt%, 5 min mixing time, magnification: 1000X, scale bar: 20 μm **g)** PLA/MOF 5wt%, 5 min mixing time, magnification: 1600X, scale bar: 20 μm **h)** PLA/MOF wt%, 5 min mixing time, magnification: 1600X, scale bar: 20 μm **i)** PLA/MOF 5wt%, 5 min mixing time, magnification: 2500X, scale bar: 10 μm

4.9 FTIR Spectrophotometer

An FTIR transmission graph of the PLA and MOF blends at wt% of 1, 3 and 5 is shown in Figure 4-12. The MOF used for the experiment was Basolite™ C300 (containing copper benzene-1,3,5-tricarboxylate). According to Robinson *et.al,*[4] the benzene rings shows a characteristic peak between 1500 to 2000cm^{-1} which corresponds to the C=C stretching. The PLA/MOF blend at 1 and 3% loading did not show any distinct peak in the fingerprint region for the benzene ring. However, the PLA/MOF composite at 5% loading shows an absorption at 1537cm^{-1}, corresponding to the C=C stretching. The peak assignments of Figure 4.12 are shown in Table 4.10.

Figure 4.12 IR Spectra of PLA, PLA + 1% MOF, PLA + 3% MOF, and PLA +5% MOF ("For interpretation of the references to color in this and all other figures, the reader is referred to the electronic version of this thesis.")

Table 4.10 FTIR absorption bands of PLA/MOF composite films

Wavenumber cm^{-1}	Assignment	Wavenumber cm^{-1}	Assignment
3502	-OH Stretch(free)	1263	-C=O bend
2993(asym),2945(sym),2879	-CH Stretch	1182,1134	-C-O- Stretch
1755	-C=O Carbonyl stretch	1056	-OH bend
1537	-C=C aromatic ring stretch	954	-CH3 rocking
1450	-CH3 bend	867,756,705	-C-C- stretch
1382,1355	-CH- Sym,, Asym. bend		

4.10 Ultraviolet/Visible Spectroscopy

The UV/Visible spectrum of the film samples shown in Figure 4.13 give a distinct absorbance and transmittance peak in the 190 to 800 nm range (UV A, B, C and visible range). The MOF (Basolite™ C300) is Cyan (Blue + Green) in color due to the presence of copper (Cu) ions in the matrix. The cyan color showed an increased absorbance in the red region (620 – 750 nm). On the other hand, the transmittance is greater in the blue and green region (450-570 nm). It is also evident from the spectra that as the percentage of MOF increases, the transmittance decreases.
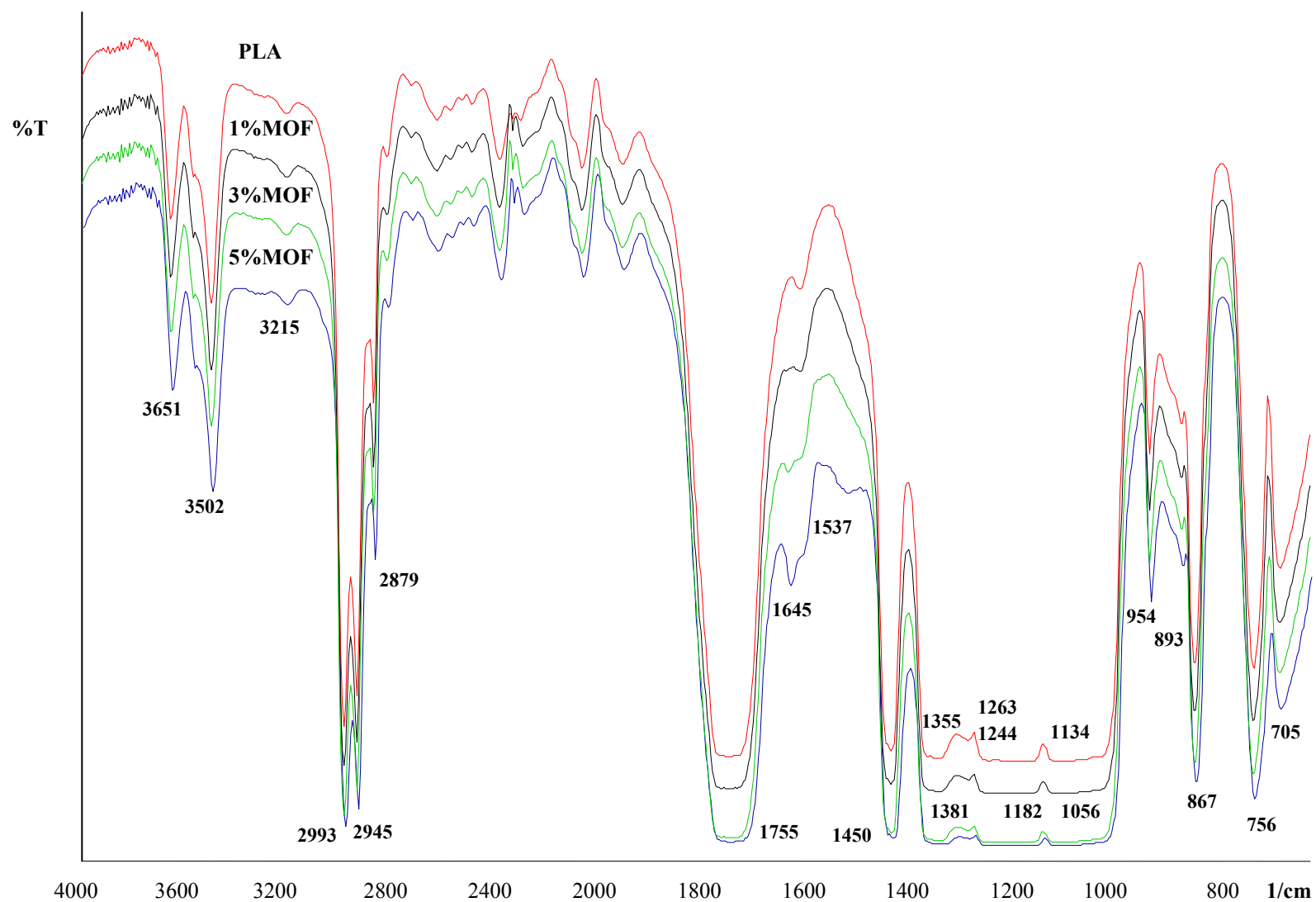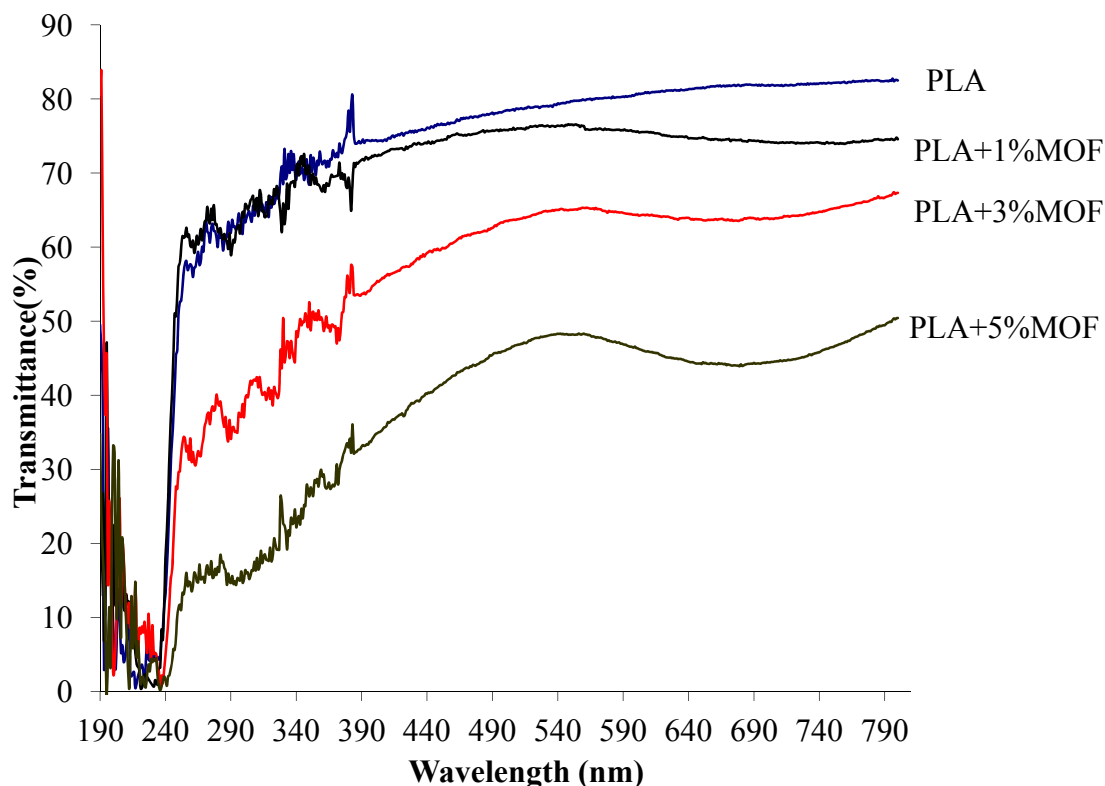
Figure 4.13 UV spectra of PLA, PLA + 1% MOF, PLA + 3% MOF, and PLA + 5% MOF ("For interpretation of the references to color in this and all other figures, the reader is referred to the electronic version of this thesis.")

4.11 Colorimeter

The L^* a^* b^* and ΔE values of the PLA and MOF blends at wt% of 1, 3 and 5 are shown in Table 4.11. The higher the L value, the lighter the samples are. As the percentage of MOF increases (i.e. 1, 3, and 5%), the L^* values of the film samples decrease indicating that the clarity of the film samples diminishes as the percentage of MOF increases. The decreasing a^* values in the case of 1, 3, and 5% loading indicate that the addition of MOF gives a green tone to the film. The positive b^* values indicate the presence of yellow color in the samples. The increasing b^* values in the case of 1, 3,

and 5% loading indicates the addition of MOF gives a yellow tone to the film. The ΔE

value is an indicative of magnitude of the difference in color with respect to PLA. The

ΔE value increases significantly as the percent of MOF increases. The above $L*$ $a*$ $b*$

and ΔE indicates that the addition of MOF (Cyan in color due to the presence of copper)

changes the color of the sample to cyan (blue + yellow).

Table 4.11 CIE $L*a*b*$ Values of for PLA and MOF samples

Material	$L*$	$a*$	$b*$	ΔE
PLA	92.5 ± 0.1^a	-1.1 ± 0.01^a	0.9 ± 0.03^a	N/A
PLA+1%MOF	87.8 ± 1.2^b	-3.7 ± 0.5^b	2.3 ± 0.4^b	5.5^a
PLA+3%MOF	81.7 ± 1.7^c	-7.2 ± 0.7^c	2.4 ± 0.1^b	12.5^b
PLA+5%MOF	76.8 ± 1.3^d	-9.1 ± 0.6^d	2.2 ± 0.2^b	17.7^c

Note: Values are represented as averages ± standard deviation. Values with different
superscript letters in the same column is significantly different at $\alpha = 0.05$ (Tukey –
HSD)

4.12 Dynamic mechanical analyzer (DMA)

The heat deflection temperature (HDT) and T_g obtained from Tan Δ are shown in

Table 4.12 for run 1 and 2 of the PLA and PLA/MOF composite. The HDT and T_g by

Tan Δ do not show any significant difference between PLA and PLA/MOF composites

within the runs. In run 1, even at 5% loading of MOF, HDT and T_g by TanΔ were found

to be 54.7 and 64.7 ºC in comparison to the HDT and T_g by TanΔ of 53.4 and 65.4 ºC for

the control (PLA). Significant differences were found between samples in runs 1 and 2

samples. These differences can be attributed to the differences in the processing

conditions of the extruder, and also due to the inherent variability of the testing machines.

The storage modulus and loss modulus of PLA/MOF composites did not change when compared to the neat PLA even at 5% wt/wt loading of MOF. The storage modulus and loss modulus of PLA and PLA/MOF composite were found to be around 3150 and 700 MPa. The study of PLA/Zeolite composites done by Yuzay et.al [3] reported that addition of 5% wt/wt of zeolite increased the storage modulus of PLA from 3100 to 3854 MPa. The loss modulus values also increased with zeolite loading. The loss modulus of PLA with 5% wt/wt zeolite reached 901 MPa when compared to pure PLA, which was about 668 MPa. The current results show that the addition of MOF does not change the dissipation capacity of PLA for vibrational energy. Figure 4.14 and 4.15 show the storage and loss modulus curves of the PLA and PLA/MOF composites.

Table 4.12 HDT and Tg by Tan delta results of PLA, PLA + 1% MOF, PLA + 3% MOF, and PLA + 5% MOF samples

Run	Treatment	HDT(^{o}C)	T_g by TanΔ(^{o}C)
1	PLA	$52.45\pm0.25^{a,A}$	$67.16\pm0.37^{a,A}$
	PLA + 1%MOF	$52.43\pm0.23^{a,A}$	$67.07\pm0.15^{a,A}$
	PLA + 3%MOF	$52.47\pm0.18^{a,A}$	$66.90\pm0.2^{a,A}$
	PLA + 5%MOF	$53.12\pm0.19^{a,A}$	$67.50\pm0.0^{a,A}$
2	PLA	$53.44\pm0.66^{a,B}$	$65.40\pm0.2^{a,B}$
	PLA + 1%MOF	$54.10\pm0.34^{a,B}$	$65.20\pm0.3^{a,B}$
	PLA + 3%MOF	$54.63\pm0.38^{a,B}$	$65.00\pm0.3^{a,B}$
	PLA + 5%MOF	$54.72\pm0.18^{a,B}$	$64.70\pm0.1^{a,B}$

Note: Values are represented as averages ± standard deviation. Values within runs with different lower-case superscript letters are significantly different at α = 0.05 (Tukey – HSD). Values between runs with different upper-case superscript letters are significantly different at α = 0.05 (Tukey – HSD).
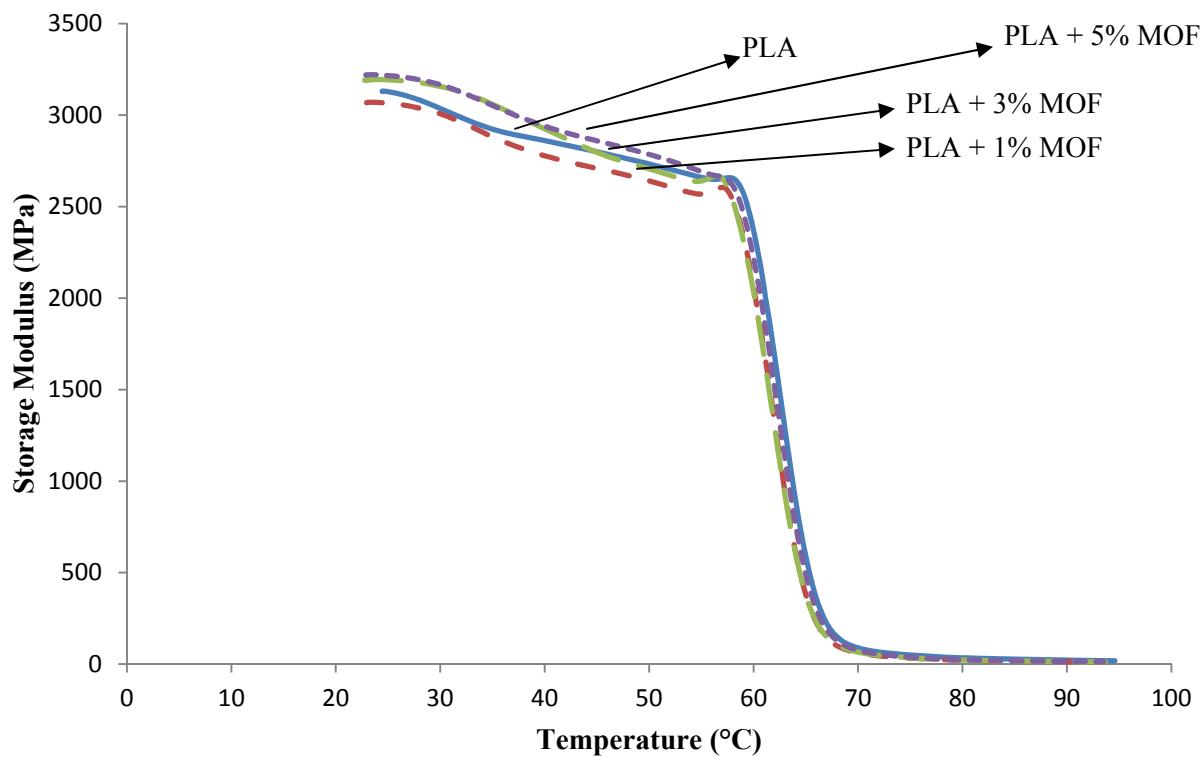
Figure 4.14 DMA Curve for Storage Modulus of PLA, PLA+1%MOF, PLA+ 3%MOF and PLA+5%MOF ("For interpretation of the references to color in this and all other figures, the reader is referred to the electronic version of this thesis.")
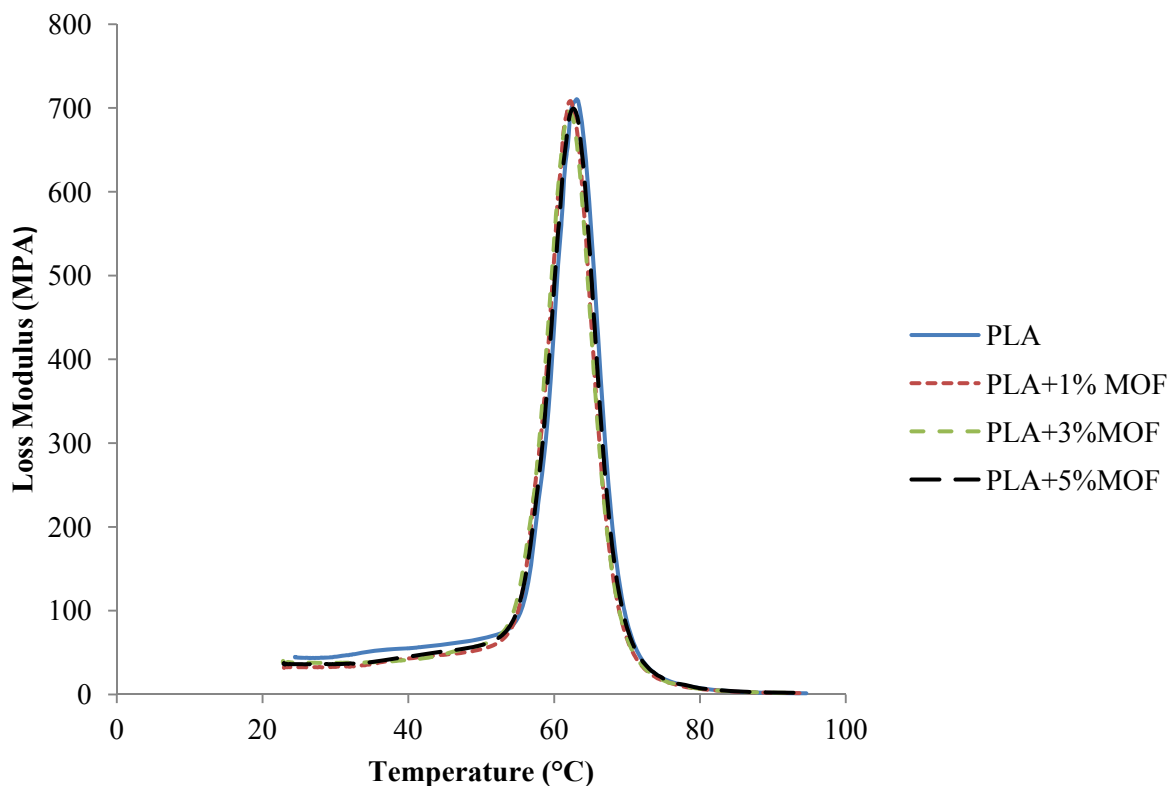
Figure 4.15 DMA Curve for Loss Modulus of PLA, PLA+1%MOF, PLA+ 3%MOF and PLA+5%MOF ("For interpretation of the references to color in this and all other figures, the reader is referred to the electronic version of this thesis.")

4.13 Differential Scanning Calorimetry

The films made by compression molding and the samples extruded from the twin screw extruder were analyzed for their thermal properties using DSC. The T_g, T_c, T_m, H_c, ΔH_m, and crystallinity of the films and extruded samples are tabulated in Tables 4.12 & 4.13. For the compression molded films the addition of MOF did not affect the glass transition temperature (T_g) and the percent crystallinity (X_c). However, there was a change in the melting temperature (T_m) and cold crystallization. The compression molded PLA and PLA/MOF composites had a T_g around 60°C.

On heating from the T_g, the PLA and PLA/MOF composites reached the cold crystallization temperature where the polymer chains oriented themselves to form crystallites. A lower cold crystallization temperature is associated with fast crystallization. The T_c of PLA was found to be 129.2±0.3°C. As the percentage of MOF increased, the cold crystallization shifted to lower temperatures (T_c = 115.0±0.8°C for PLA with 5% MOF). This reduction can be attributed to a nucleating effect caused by the addition of MOF particles in the PLA matrix. The same effect has been reported by Yuzay et al [3] upon combining PLA with zeolites to form PLA/zeolite composites.

The compression molded films, which were subjected to two thermal cycles, exhibited bimodal melting peaks for the PLA/MOF composites. The PLA/MOF composites showed melting peak T_{m1} at 149.6±0.0 °C and another peak T_{m2} at 154.9±0.2°C. Figure 4.16 shows the DSC graphs of the PLA and PLA plus 1, 3 and 5% wt/wt MOF composite films. These double melting peaks can be attributed to the presence of different crystallite structures. The T_{m1} can be attributed to β crystallites of PLA, and T_{m2} can be attributed to the α -crystallites. PLA crystallizes in three forms α, β and γ. The α-form, which is more stable than the β and γ forms, is commonly found and distinguished by 2θ values of 15, 17 and 19°, and is described by two antiparallel chains in a left-handed 10_3 helix conformation packed in a pseudoorthorhombic unit cell (a=10.6 Å, b=6.10 Å, and c=2.8 Å). [22] From Table 4.13, the addition of increasing amounts of MOF did not affect the T_{m1} & T_{m2} temperatures of the bimodal melting peaks, but the

peaks became more prominent upon increasing the amount of MOF. The low % X_c of the samples indicated a mostly amorphous sample.

In case of the thermal properties of extruded PLA and PLA plus 1, 3 and 5% wt/wt MOF composite samples (disc samples), we did not observe the decreasing cold crystallization temperature or the bimodal peaks in case of PLA/MOF composites. As seen in the Table 4.14, there was no significant difference between the T_g, T_{cc}, T_m and the X_c of the PLA and PLA/MOF composites.

Table 4.13 Thermal Properties of PLA/MOF Composites (films)

Treatment	T_g (° C)	T_c (° C)	T_{m1} (° C)	T_{m2} (° C)	H_c (J/g)	H_m (J/g)	X_c (%)
PLA	60.1±0.1[a]	129.2±0.2[a]	151.3±0.3		12.5±0.4[a]	13.9±0.2[a]	1.5±0.2[a]
PLA+1% MOF	59.8±0.2[a]	123.2±0.7[b]	149.6±0.0[a]	154.9±0.2[a]	23.9±2.2[b]	25.6±2.3[b]	1.8±0.9[a]
PLA + 3% MOF	59.2±0.1[a]	117.1±0.1[c]	148.1±0.1[a]	155.2±0.1[a]	32.9±0.6[c]	34.7±0.7[c]	1.9±0.5[a]
PLA+ 5% MOF	59.2±0.2[a]	115.0±0.8[d]	147.3±0.2[a]	154.9±0.1[a]	33.5±0.7[c]	34.9±1.2[c]	1.7±1.1[a]

Note: Values are represented as averages ± standard deviation. Values with different superscript letters in the same column is significantly different at $\alpha = 0.05$ (Tukey – HSD)

Table 4.14 Thermal Properties of PLA/MOF Composites (extruded disc samples)

Treatment	T_g (° C)	T_c (° C)	T_m (° C)	H_c (J/g)	H_m (J/g)	X_c (%)
PLA	61.0±0.2[a]	130.7±0.3[a]	152.1±0.1[a]	7.1±0.3[a]	7.9±0.4[a]	0.8±0.1[a]
PLA+1% MOF	61.1±0.2[a]	131.0±0.2[a]	152.3±0.4[a]	5.2±0.5[b]	5.9±0.4[b]	0.8±0.2[a]
PLA + 3% MOF	61.5±0.1[a]	131.4±0.2[a]	152.3±0.4[a]	4.2±0.2[c]	5.2±0.2[b]	1.2±0.2[a]
PLA+ 5% MOF	61.3±0.2[a]	131.6±0.1[a]	152.4±0.4[a]	3.8±0.2[c]	4.6±0.2[b]	0.9±0.1[a]

Note: Values are represented as averages ± standard deviation. Values with different superscript letters in the same column is significantly different at $\alpha = 0.05$ (Tukey – HSD)
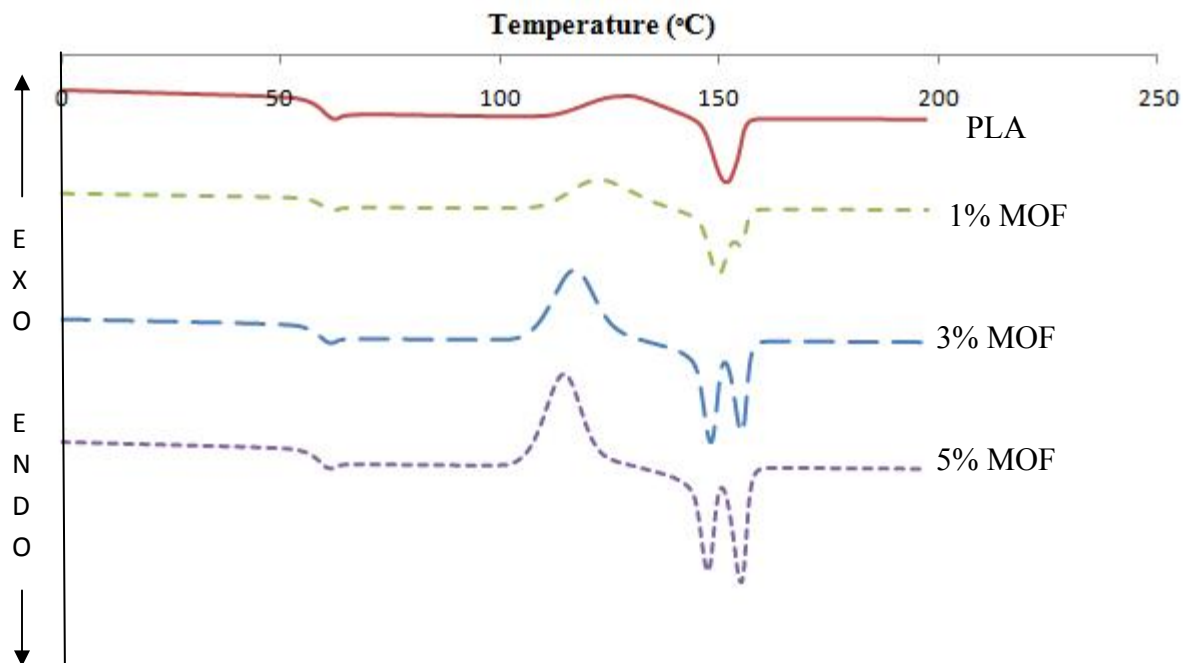
Figure 4.16 Thermograph of PLA and PLA films plus 1, 3, and 5% wt/wt MOF composites ("For interpretation of the references to color in this and all other figures, the reader is referred to the electronic version of this thesis.")

4.14 Thermal Gravimteric Analysis
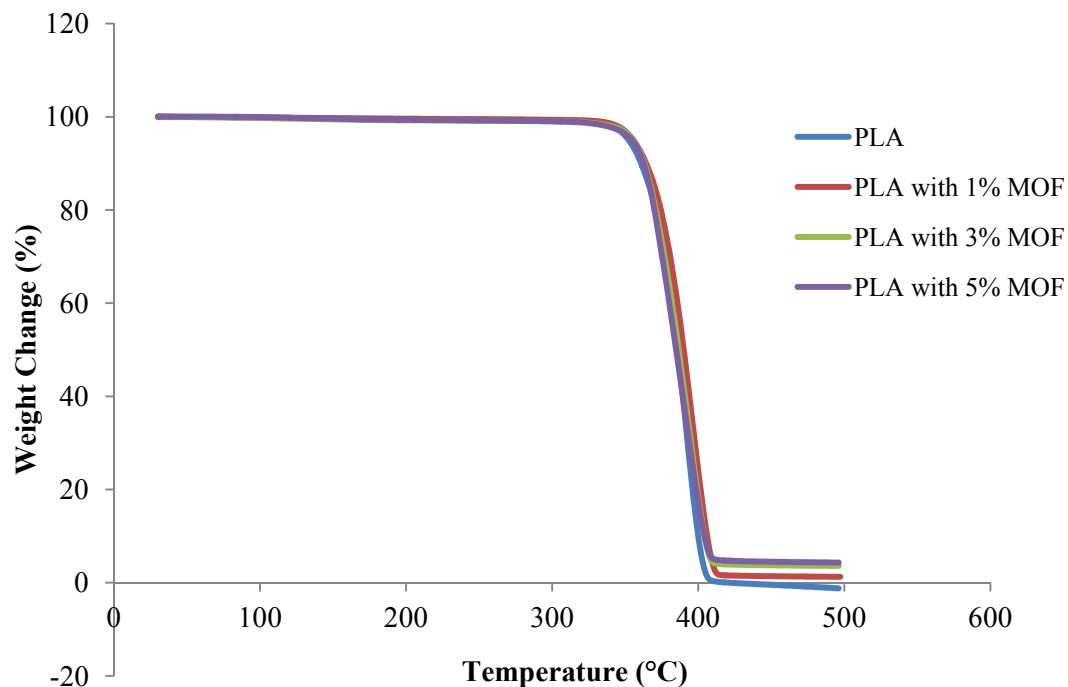
Figure 4.17 TGA curves of PLA and PLA/MOF composites ("For interpretation of the references to color in this and all other figures, the reader is referred to the electronic version of this thesis.")

Table 4.15 TGA analysis of PLA and PLA/MOF Composites

MOF content (% wt)	$T_{5\%}$ Weight loss	$T_{50\%}$ Weight loss	$T_{95\%}$ Weight loss	T_{dmax}	Weight Loss (%)
0	352	386	403	419	98.84
1	355	390	409	420	97.94
3	353	387	408	420	95.16
5	355	385	411	420	94.08

The TGA analyses of the PLA and PLA/MOF composites are shown in Figure 4.17. The onset and termination of the degradation temperature did not change between the PLA and PLA/MOF composite as shown in Table 4.15. On average, the degradation

88

started at around 310°C, and terminated at about 420°C. The weight losses of the PLA

and PLA/MOF composite films were found to be 98.84, 97.94, 95.16 and 94.08 for the

control and addition of 1, 3, and 5% MOF, respectively. Although the PLA/MOF

composite sample should contain 1, 3 and 5% of MOF, the TGA results did not agree

with this, indicating that the MOF also degrades at the same temperature as PLA. A

thermogram of the degradation of MOF is presented in figure 4.18.
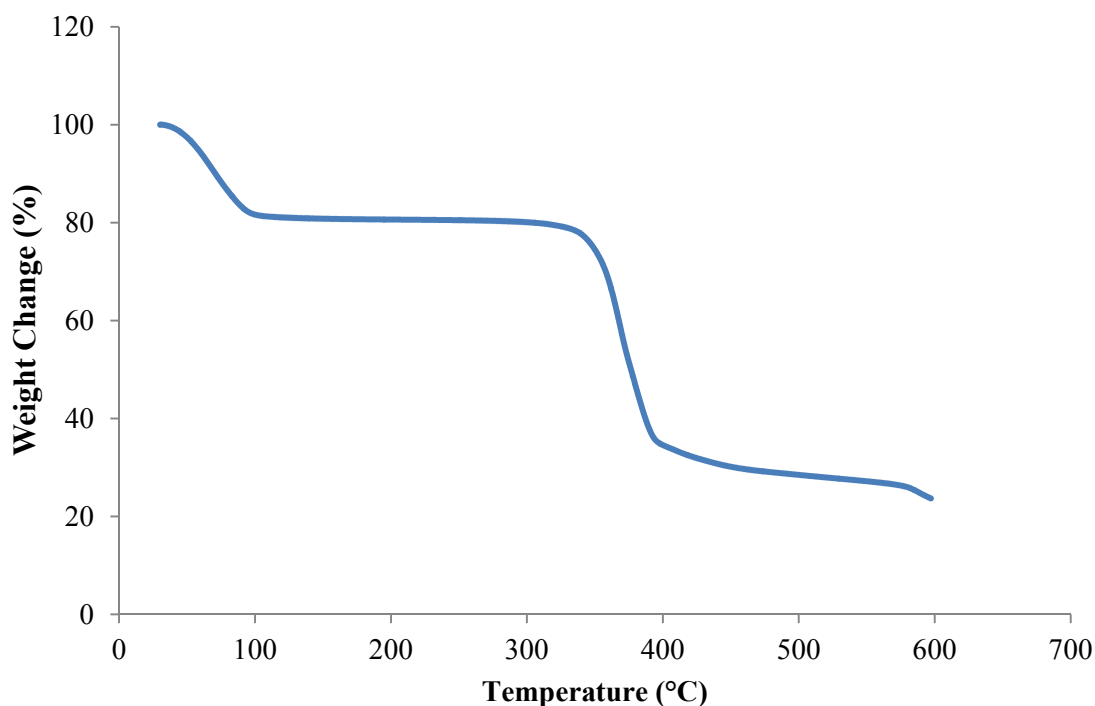
Figure 4.18 TGA curve of MOF activated at 200°C in vacuum

As shown in figure 4-18, the first weight loss from 30 to 100°C can be attributed

to the evaporation of water bound in the pores of the MOF, and then the MOF started to

degrade at 310 to around 400˚C, the same temperature as PLA. But in the case of

PLA/Zeolite composites, the zeolite does not decompose at these higher temperatures, so

the amount of zeolite in the extruded PLA samples could be determnined by TGA. The

addition of MOF does not affect the degradation temperature of PLA. Yuzay et al. [3] reported a slight reduction in decomposition temperature when zeolite is added to the PLA matrix. A similar reduction in degradation temperature is reported for PLA when titanium oxide and clay nanoparticles were added to the PLA. [23 - 26] So, the actual amount of MOF in PLA was determined by ICP-MS as described in section 3.2.2. The weight loss of the MOF is about 80% and the 5%, 50% reduction temperature and T_{dmax} are about 58°C, 377°C and 597°C respectively.

4.14 Izod impact Testing Machine

Stiffness and toughness are critical properties in the performance of composites and its applications. Notched impact strength is related to the toughness of a polymer. The notched impact strength of the PLA and the PLA/MOF composites are shown in Table 4.16. Two runs (i.e. extrusion using twin screw extruder) for each treatment (i.e. 1, 3, 5 % wt/wt) were conducted to analyze the difference in impact strength between the PLA and PLA/MOF composite. According to run 1, there was no significant difference between PLA and 1% wt/wt MOF loading, but it found that there was a significant difference for 3 and 5% wt/wt MOF loading when compared to the PLA and 1% MOF loading. In run 2 there was a significant difference between PLA and PLA/MOF composite (i.e. 1, 3 and 5%). The results from runs 1 and 2 were different. We can conclude from run 1 and run 2 that there is a difference in impact strength between the control (PLA) and PLA + 3 and 5% MOF. However, further testing is needed to determine the differences between PLA + 1% MOF. Huda *et al.* [5] reported the impact strength properties of PLA/wood fiber composites. The addition of wood decreased the

90

impact strength of PLA from 25.7 to 21.9 J/m. In this study, the addition of MOF

significantly increased the impact strength and toughness of the PLA+MOF samples. The

increased impact strength is due to the homogenous distribution of MOF in the PLA

matrix. The surface area of the MOF is able to absorb much of the impact energy, and the

void between the MOF and PLA matrix acts as a cushion , which absorb the impact force.

Table 4.16 Impact strength of PLA and PLA/MOF composites

RUN	Specimen	Impact Strength (J/m)
1	PLA	$26.76 \pm 1.27^{a.A}$
	PLA + 1%MOF	$27.30 \pm 0.76^{a,A}$
	PLA + 3%MOF	$31.18 \pm 1.17^{b,A}$
	PLA + 5%MOF	$31.11 \pm 3.06^{b,A}$
2	PLA	$26.80 \pm 0.45^{a,A}$
	PLA + 1%MOF	$28.31 \pm 0.47^{b,A}$
	PLA + 3%MOF	$28.42 \pm 0.72^{b,B}$
	PLA + 5%MOF	$29.47 \pm 0.92^{b,A}$

Note: Values are represented as averages ± standard deviation. Values within runs with different lower-case superscript letters are significantly different at $\alpha = 0.05$ (Tukey – HSD). Values between runs with different upper-case superscript letters are significantly different at $\alpha = 0.05$ (Tukey – HSD).

4.15 Tensile test

Table 4.17 shows the tensile strength, modulus of elasticity, strain at yield, and

strain at break of the PLA and PLA/MOF composites. Mechanical properties were

assessed for samples made from three runs in order to account for the variability

associated with the extrusion of the samples. Tensile strength of the samples decreased

as the percentage of the MOF in the sample increased. For example, run 2 samples had

tensile strength of the PLA of about 9.52±0.26 kPsi while PLA with 5% MOF had tensile

strength about 6.95±0.19 kPsi, which was found to be significantly different. The

decrease in tensile strength can be attributed to the poor interfacial adhesion between the

MOF and PLA, as predicted by the solubility parameter measurements. Yuzay *et. al.*, [6]

reported that adding zeolite to a PLA matrix did not change the tensile strength of the

composite sample significantly. This was attributed to the good interfacial adhesion

between PLA and zeolite. It was found that the modulus of elasticity was not

significantly difference between PLA and PLA/MOF composites for run 1. The samples

tested from run 2 exhibited a significant difference between PLA and PLA/MOF

composites. The difference between the runs could be due to the variability in the mixing

during the extrusion.

Table 4.17 Mechanical Properties of PLA/MOF Composite

Run	Treatment	Tensile Strength (Kpsi)	Modulus of Elasticity (Kpsi)	Strain at yield (%)	Strain at Break (%)
1	PLA	$9.32\pm0.26^{a,A}$	$479.53\pm11.14^{a,A}$	$2.45\pm0.21^{a,A}$	$1.17\pm0.30^{a,A}$
	PLA+1%MOF	$8.69\pm0.19^{b,A}$	$488.16\pm30.73^{a,A}$	$2.46\pm0.21^{a,A}$	$>170^{b,A}$
	PLA+3%MOF	$8.47\pm0.36^{c,A}$	$468.32\pm41.60^{a,A}$	$2.68\pm0.15^{a,A}$	$>170^{b,A}$
	PLA+5%MOF	$6.95\pm0.20^{d,A}$	$490.39\pm32.26^{a,A}$	$2.28\pm0.16^{a,A}$	$>170^{b,A}$
2	PLA	$9.52\pm1.49^{a,A}$	$451.71\pm22.72^{a,A}$	$2.42\pm0.32^{a,A}$	$3.58\pm0.33^{a,A}$
	PLA+1%MOF	$8.92\pm1.22^{b,A}$	$400.52\pm20.23^{b,B}$	$2.54\pm0.10^{a,A}$	$>170^{b,A}$
	PLA+3%MOF	$8.3\pm1.30^{c,A}$	$400.70\pm22.36^{b,B}$	$2.54\pm0.12^{a,A}$	$>170^{b,A}$
	PLA+5%MOF	$7.66\pm0.72^{d,A}$	$436.01\pm18.36^{b,A}$	$2.37\pm0.04^{a,A}$	$>170^{b,A}$

<u>Note:</u> Values are represented as averages ± standard deviation. Values within runs with
different lower-case superscript letters are significantly different at α = 0.05 (Tukey –
HSD). Values between runs with different upper-case superscript letters are significantly
different at α = 0.05 (Tukey – HSD).

As the MOF is introduced into the PLA matrix, the strain at break of the samples increased by 2 orders of magnitude. For example, pure PLA extension at break was about 3.6±0.3 % but the addition of 1% wt/wt MOF increased the strain at break to greater than 170 % (run 2). A laser beam was used as a strain detector in the UTS machine. Due to necking of the samples (which is common in small dumb-bell shaped samples), the laser could not exactly quantify the ultimate extension of samples after extension of about 170 %. In order to unify the data, the MOF sample extension at break is reported as >170%. The addition of starch to PHB increased the impact strength of the polymer to 130% at 25 wt% loading, but the impact strength decreased significantly as the amount of starch added to the PHB increased. The same effects were observed when flax fiber was added to HDPE to form a composite material. The addition of starch and flax fiber to the polymer matrix increases the tensile strength and decrease the elongation of break of the polymer samples. [27, 28] But, the addition of MOF to the PLA matrix increased the elongation of break and decreased the tensile strength. This is due to poor interfacial addition of MOF with the PLA matrix, which resulted in void formation in the extruded samples. These voids resulted in the reduced tensile strength, which in turn increased the flexibility of the PLA/MOF composite samples and the elongation at break. In the case of PLA/zeolite composites, the addition of zeolite decreased the elongation at break from 10.96 to 6.68 % and slightly increased the tensile strength due to high interfacial adhesion between PLA and zeolite matrix. [6]

4.16 Barrier Properties:

The permeability to water and oxygen plays a major role in determining polymer performance and application and the design of a functional membrane. The water vapor permeability (WVP) and oxygen permeability (OP) in $kg.m.m^{-2}s^{-1}Pa^{-1}$ of PLA and PLA/MOF composite samples are shown in Table 4.17. In case of the WVP, there was no significant difference between the PLA and PLA/MOF composites between runs 1 and 2, and also between the treatments within the runs. This indicates that the addition of MOF did not increase or decrease the permeability of PLA to water. The same trend was followed in case of OP, where the addition of MOF did not change the PLA permeability to oxygen. Significant differences were not found between the OP values for runs 1 and 2.

Table 4.17 Barrier properties of PLA/MOF Composites

Run	Material - ID	WVP (kg-m/m²skpa) x10⁻¹³	OP (kg-m/m²skpa) x10⁻¹³
1	PLA	$3.1\pm0.5^{a,A}$	$4.9\pm0.5^{a,A}$
	PLA+1%MOF	$2.5\pm0.5^{a,A}$	$4.3\pm0.2^{a,A}$
	PLA+3%MOF	$2.5\pm0.01^{a,A}$	$4.0\pm0.3^{a,A}$
	PLA+5%MOF	$2.5\pm0.5^{a,A}$	$4.8\pm0.7^{a,A}$
2	PLA	$2.4\pm0.2^{a,A}$	$5.0\pm0.4^{a,A}$
	PLA+1%MOF	$2.5\pm0.6^{a,A}$	$4.7\pm0.3^{a,A}$
	PLA+3%MOF	$2.1\pm0.2^{a,A}$	$4.6\pm0.4^{a,A}$
	PLA+5%MOF	$2.5\pm0.3^{a,A}$	$4.6\pm0.9^{a,A}$

Note: Values are represented as averages ± standard deviation. Values within runs with different lower-case superscript letters are significantly different at $\alpha = 0.05$ (Tukey – HSD). Values between runs with different upper-case superscript letters are significantly different at $\alpha = 0.05$ (Tukey – HSD).

4.17 Sorption

The sorption isotherm represents the relationship between the amount of water vapor amount in the environment and the water activity of a material at a constant temperature. Measurement of the sorption isotherm in polymer membranes is important for many industrial applications such as fuel cells, gas separation, packaging, and drug delivery systems. Compounding PLA with highly porous MOF particles should have greatly affected the polymer sorption capacity for water. To study the sorption isotherm of the PLA and PLA/MOF composites, PLA and PLA +5%wt MOF samples were subjected to various relative humidity levels and the sorption isotherms of the films were obtained. Table 4.18 depicts the weight change (%) (i.e., grams of water/gram of dry polymer x 100) of the PLA and PLA with 5% MOF composite films at various relative humidity.) Figure 4.17 shows the sorption isotherm of PLA and PLA with 5% MOF composite film. The addition of MOF increased the adsorption capacity of the polymer to water. The sorption capacity of the MOF composite films to water started increasing from 10% RH at 0.1 ± 0.0 % through 90% RH at 1.6 ± 0.4 %, respectively. Roughly the sorption capacity of the films modified with MOF doubled compared to the pure PLA. This indicates the MOF has greater affinity to water molecules due to its porous nature. The water molecules started accommodating into the pores of the MOF. The kinetic diameter of a water molecule is 0.27 nm and thus gets easily accommodated in the 1.86 nm pores of MOF. The water absorption of neat PLA coincides well with the results reported by Wang *et.al.* [29] Also the higher variability of PLA/MOF composite film at 90% RH could be due to the uneven distribution of MOF in the PLA matrix of the

95

pressed film, and the saturation of the film with water producing varied results between

replicates.

Table 4.18 Weight change of PLA and PLA/MOF composite between 0 and 90% RH

RH(%)	Weight Change (%)	
	PLA	**PLA with 5% MOF**
0	$0.00\pm0.00^{a,A}$	$0.00\pm0.00^{a,A}$
10	$0.03\pm0.01^{a,A}$	$0.09\pm0.00^{b,B}$
30	$0.16\pm0.02^{b,A}$	$0.31\pm0.01^{c,B}$
40	$0.21\pm0.02^{c,A}$	$0.40\pm0.02^{d,B}$
50	$0.26\pm0.02^{d,A}$	$0.46\pm0.04^{e,B}$
60	$0.33\pm0.01^{e,A}$	$0.59\pm0.04^{f,B}$
70	$0.43\pm0.03^{f,A}$	$0.78\pm0.12^{g,B}$
80	$0.58\pm0.02^{g,A}$	$1.12\pm0.33^{h,B}$
90	$0.76\pm0.03^{h,A}$	$1.59\pm0.40^{i,B}$

Note: Values are represented as averages ± standard deviation. Values within runs with different lower-case superscript letters are significantly different at $\alpha = 0.05$ (Tukey – HSD). Values between runs with different upper-case superscript letters are significantly different at $\alpha = 0.05$ (Tukey – HSD).
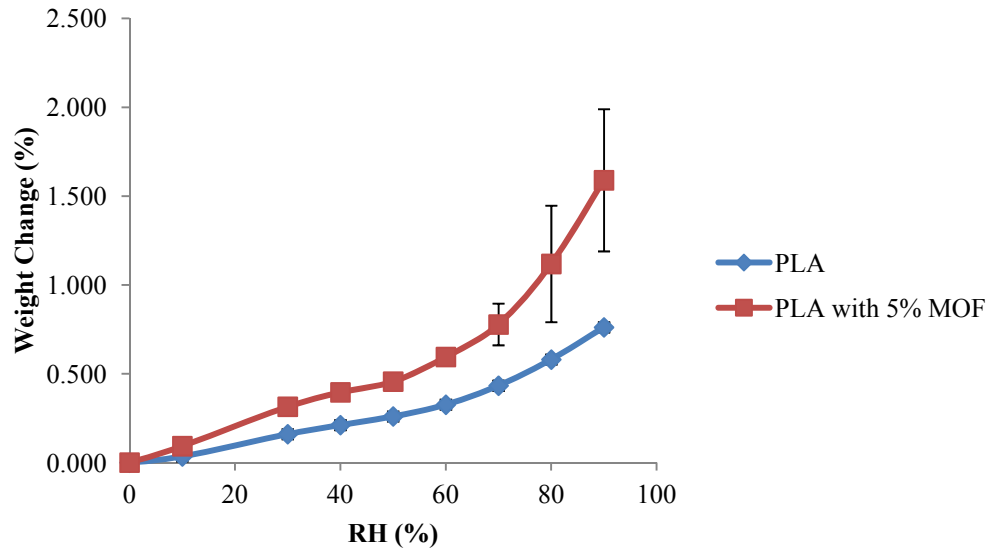

Figure 4.19 Water sorption of PLA and PLA+5%MOF composite at 23°C and 40%RH ("For interpretation of the references to color in this and all other figures, the reader is referred to the electronic version of this thesis.")

4.18 Desorption

The desorption isotherm is the curve used to determine the behavior of the material while drying. Since films modified with MOF adsorbed an increased amount of water, a desorption isotherm was measured to analyze its drying behavior. The desorption isotherm of PLA with 5% MOF composite films is shown in Figure 4.18. As expected the sorption and desorption curves do not follow the same trend due to the hysteresis effect typical of many desorption isotherms for foods and polymers for the experimental time period. Since the MOF does not have any dead volume (the amount of solvent adsorbed will be desorbed without any loss), the hysteresis effect is mainly produced by PLA. The same effect is also reported by Hsu *et.al.,* [30] for all of the poly(methyl methacrylate) PMMA blends. Because of the limited amount of data, it was not possible to conclude whether the hysteresis in the PLA/MOF blends is time dependent or not. Schult and Paul [31] also found a hysteresis effect for blends of poly(vinyl pyrrolidone) and polysulfone.
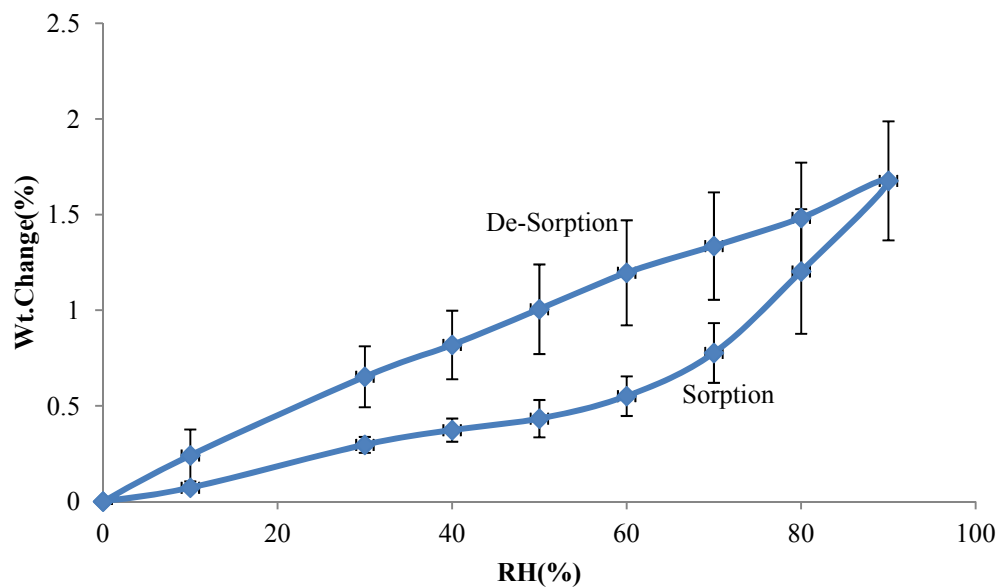
Figure 4.20 Water desoprtion isotherm of PLA + 5% MOF ("For interpretation of the references to color in this and all other figures, the reader is referred to the electronic version of this thesis.")

REFERENCES

REFERENCES

1. H. Pehlivan, "*Preparation and characterization of polypropylene based composite films*". M.S. Thesis, İzmir Institute of Technology, Chemical Engineering Department İzmir, Turkey; 2001.

2. S. Sinha Ray, K. Yamada, M. Okamoto, K. Ueda, "*Biodegradable Polylactide/Montmorillonite Nanocomposite*" Journal of Nanoscience and Nanotechnology, 3(6), 2003, pp. 1-5.

3. I. Yuzay, R. Auras, S. Selke, "*Poly(lactic acid)/ Aluminum Oxide Composites Fabricated by Sol-Gel and Melt Compounding Processes*", Macromolecular Materials and Engineering, 295, 2010, pp. 283-292.

4. J. W. Robinson, E. M. Skelly Frame, G. M. Frame II, "*Undergraduate instrumental analysis*", sixth edition, Marcel Dekker publications, New York, 2005.

5. M.S. Huda, L.T. Drazal, A.K. Mohanty, M. Misra, "*Wood fiber reinforced poly(lactic acid) composites*" 5th annual SPE automotive composition conference, Troy, MI, USA , September 12-14, 2005.

6. I.E. Yuzay, R. Auras, S. Selke, "*Poly(lactic acid) and Zeolite Composites Prepared by Melt Processing: Morphological and Physical-Mechanical Properties*", Journal of Applied Polymer Science, 115 (4), 2009, pp.2262-2270.

7. E. Schwach, L. Averous, "*Starch-based biodegradable blends: morphology and interface properties*". Polymer International, 53(12), 2004, pp.2115-2124.

8. P. S. Wheatley, A. C. McKinlay, R. E. Morris, "A comparison of zeolites and metal organic frameworks as storage and delivery vehicles for biologically active nitric oxide", *Studies in surface science and catalysis*, 174(1), 2008, pp.441-446.

9. R. C. Huxford, J. D. Rocca, W. Lin, "Metal-organic frameworks as potential drug carriers", *Current opinion in chemical biology*, 14(2), 2010, pp. 262-268.

10. S.R. Wasserman, Y.T. Tao, G.M. Whitesides, "*Structure and reactivity of alkylsiloxane monolayers formed by reaction of alkyltrichlorosilanes on silicon substrates*", Langmuir, 5(4), 1989, pp. 1074-1087.

11. M. Fuji, H. Fujimori, T. Takei, T. Watanabe, M. Chikazawa, "*Wettability of glass-bead surface modified by trimethylchlorosilane*", Journal of Physical Chemistry, 102(51), 1998, pp.10498-10504.

12. D.L. Angst, G.W. Simmons, "*Moisture absorption characteristics of organosiloxane self-assembled monolayers*", Langmuir, 7(10), 1991, pp.2236-2242.

13. G. Buckton, J.M. Newton, "*Assessment of the wettability of powders by use of compressed powder discs*",   Powder Technology, 46, 1986, pp.201-208.

14. M. Jia, K.V. Peinemann, R.D. Behling, "*Molecular sieving effect of the zeolite-filled silicone rubber membranes in gas permeation*", Journal of Membrane Science, 57, 1991, pp.289-296.

15. J.M. Duval, "*Adsorbent filled polymeric membranes*", Ph.D thesis. The Netherlands, University of Twente, 1995.

16. G. Clarizia, C. Algieri, E. Drioli, "*Filler-polymer combination: a route to modify gas properties of a polymeric membrane*", Polymer, 45, 2004, 5671-5681.

17. Y. Li, T.S. Chung, C. Cao, S. Kulprathipanja, "*The effects of polymer chain rigidification, zeolite pore size and pore blockage on polyethersulfone (PES)-zeolite A mixed matrix membranes*", Journal of Membrane Science, 45, 2005, pp.260.

18. G. Clarizia, C. Algieri, A. Regina, E. Drioli, "*Zeolite based composites PEEK-WC membranes: Gas transport and surface properties*", Microporous and Mesoporous Materials, 115, 2008, pp.67-74.

19. C.M. Hansen, "*Hansen Solubility Parameters – A user's handbook*", CRC Press, 2007.

20. L.T. Lim, R. Auras, M. Rubino, "*Processing technologies for poly(lactic acid)*", Progress in Polymer Science, 33(8), 2008, pp. 820-852.

21. K.S.W. Sing, "*Physisorption of Nitrogen by Porous Materials*", Journal of Porous Materials, 2, 995, pp.5-8.

22. D. Brizzolara, H.J. Cantow, K. Diderichs, E. Keller, A.J. Domb, "*Mechanism of the Stereocomplex Formation between Enantiomeric Poly(lactide)s*", Macromolecules, 29, 1996, pp. 191-197.

23. N. Nakayama, T. Hayashi, "*Preparation and characterization of poly(L-lactic acid)/TiO2 nanoparticle nanocomposite films with high transparency and efficient photodegradability*", Polymer Degradation and Stability, 92, 2007, pp. 1255-1264.

24. D.F. Wu, L. Wu, L.F. Wu and M. Zhang, "*Rheology and thermal stability of polylactide/clay nanocomposites*", Polymer Degradation and Stability, **91,** 2006, pp. 3149–3155.

25. J. Chang, Y.U. An, G.S. Sur, "*Poly(lactic acid) nanocomposites with various organoclays: I—thermomechanical properties, morphology, and gas permeability*", Journal of Polymer Science, Part B: Polymer Physics, 41(1), 2003, pp.94–103.

26. N. Ogata, G. Jimenez, H. Kawai and T. Ogihara, "*Structure and thermal/mechanical properties of poly(l-lactide)-clay blend*", Journal of Polymer Science, Part B: Polymer Physics, 35(2), 1997, pp.389-396.

27. D. Erkske, I. Viskere, A. Dzene, V. Tupureina, L. Savenkova, "*Biobased polymer composites for films and coatings*", Proceedings of the Estonian Academy of Science. Chemistry, 55(2), 2006, pp.70-77.

28. X. Li, L.G. Tabil, S. Panigrahi, W.J. Crerar, " *Processing Flax Fiber-reinforced Polymer Composites by Injection Molding*", The Canadian society for engineering in agricultural, food and biological systems, Winnipeg - Manitoba, June 26-29, 2005.

29. H. Wang, X.Z. Sun and P. Seib, "*Strengthening blends of poly(lactic acid) and starch with methylenediphenyl diisocyanate*", *Journal of Applied Polymer Science,* **82,** 2001, pp. 1761–1767.

30. W.P. Hsu, R.J. Li, A.S. Myerson, T.K. Kwei, "*Sorption and diffusion of water vapour in hydrogen-bonded polymer blends*", Polymer, 34(3), 1993, pp. 587-603.

31. K. A. Schult and D. R. Paul, "*Water sorption and transport in blends of poly(vinyl pyrrolidone) and polysulfone*", Journal of Polymer Science Part B: Polymer Physics, 35(4), 1997, pp.655-674.

CHAPTER 5. CONCLUSION

Poly(lactic acid) (PLA), resin and metallic organic framework (MOF) were successfully compounded in a twin screw extruder in batches of 10 g, and rectangular, disc and dumb-bell shaped samples were prepared in the amounts of 1, 3 and 5% wt/wt. With these samples the structural, physical, optical, thermal, thermo-mechanical, mechanical and sorption properties of the PLA/MOF composites were analyzed.

Based on the contact angle measurements, the theoretical work of adhesion and positive spreading coefficient indicated that MOF might disperse well in PLA. But, the higher Relative Energy Difference (RED) of the solubility parameter study indicates otherwise suggesting that MOF may not disperse well with the PLA. In order to resolve these opposite findings, the interfacial adhesion of PLA and MOF was inspected using SEM. The SEM results revealed voids at the interface of PLA and MOF. From these visual pictures, it was clear that there was existed a poor interfacial adhesion between PLA and MOF.

The FTIR, UV and colorimetric studies showed selected absorption at particular wavelengths indicated the presence of MOF in the PLA/MOF composites. The DMA results revealed that the heat deflection temperature (HDT), storage modulus, loss modulus and Tan Δ of the PLA/MOF composites did not change when compared to the neat PLA samples. The DSC results of the PLA/MOF composite films showed two significant melting peaks, which can be attributed to the presence of different crystallite structures. The T_{m1} can be attributed to β-crystallites of PLA, and the T_{m2} can be attributed to the α-crystallites. These different crystallite structures (varied lamella

structures and spherulite size) were formed during cooling in the compression molding of PLA/MOF composite films.

The mechanical properties of the PLA/MOF composites samples changed significantly. The Izod impact strength of the PLA/MOF composite samples increased up to 15% when compared to the control (PLA sample). The tensile strength of the PLA/MOF composites decreased as the amount of MOF in the PLA samples increased. The brittleness of the PLA/MOF composite sample decreased as the amount of MOF in the PLA increased. The elongation at break (break strain) of the PLA/MOF composite samples was up to 170%, compared to about 2 % for the PLA samples.

The mass transfer properties of the PLA/MOF composite were evaluated. The permeability of PLA/MOF composite films to oxygen and water did not change when compared to the neat PLA film. However, the sorption capacity of the PLA/MOF composite films increased up to two fold at each relative humidity to which they were exposed. This shows that the addition of MOF significantly increased the sorption capacity of the PLA films. The sorption and desorption curves of the PLA/MOF composite films showed the typical hysteresis present in polymers.

Future Work

PLA and MOF composites were successful produced, which resulted in an invention disclosure form and a pending patent application. However, many details and new research questions arose during this work. Some of future topics to further investigate are:

1. The compatibility of the Cu-MOF with PLA is not proven to be good from the compatibility results between the PLA matrix and MOF. There are four types of

MOF currently available in the market 1. Cu-based, 2. Ag- based, 3. Zn-based, and 4. Fe-based. Silver based zeolites were proven to have a good compatibility with PLA in previous studies. So, in order to increase the interfacial between PLA and MOF the silver based MOF can be used with PLA. In addition, the compatibility of the PLA with the other types of MOFs (Zn, Ag, Fe based) should be studied and their properties evaluated.

2. The sorption and desorption properties to water were evaluated in this research. In order to use these membranes for packaging, the sorption properties of the PLA/MOF composite film to different solvents such as d-limonene, ethyl acetate, and acetaldehyde should be studied.

3. MOF structures can be tailored; therefore, the interfacial adhesion of PLA with MOF after modifying the MOF structure may be increased.

4. Since the thickness profile of the compression-molded film was not completely uniform, there might be little variation in the permeability results of the PLA/MOF composite film to water and oxygen. In order to reduce this variation the PLA/MOF composite film can be cast instead of compression molding.